

Magnetic Energy and Helicity Budgets in the Active-Region Solar Corona. I. Linear Force-Free Approximation

Manolis K. Georgoulis & Barry J. LaBonte[†]

*The Johns Hopkins University Applied Physics Laboratory,
11100 Johns Hopkins Rd. Laurel, MD 20723-6099, USA*

ABSTRACT

We self-consistently derive the magnetic energy and relative magnetic helicity budgets of a three-dimensional linear force-free magnetic structure rooted in a lower boundary plane. For the potential magnetic energy we derive a general expression that gives results practically equivalent to those of the magnetic Virial theorem. All magnetic energy and helicity budgets are formulated in terms of surface integrals applied to the lower boundary, thus avoiding computationally intensive three-dimensional magnetic field extrapolations. We analytically and numerically connect our derivations with classical expressions for the magnetic energy and helicity, thus presenting a so-far lacking unified treatment of the energy/helicity budgets in the constant-alpha approximation. Applying our derivations to photospheric vector magnetograms of an eruptive and a noneruptive solar active regions, we find that the most profound quantitative difference between these regions lies in the estimated free magnetic energy and relative magnetic helicity budgets. If this result is verified with a large number of active regions, it will advance our understanding of solar eruptive phenomena. We also find that the constant-alpha approximation gives rise to large uncertainties in the calculation of the free magnetic energy and the relative magnetic helicity. Therefore, care must be exercised when this approximation is applied to photospheric magnetic field observations. Despite its shortcomings, the constant-alpha approximation is adopted here because this study will form the basis of a comprehensive nonlinear force-free description of the energetics and helicity in the active-region solar corona, which is our ultimate objective.

Subject headings: MHD — Sun: atmosphere — Sun: chromosphere — Sun: corona — Sun: magnetic fields — Sun: photosphere

[†]Deceased October 24, 2005

1. Introduction

The magnetic origin of solar eruptions has been established over the past several decades of solar research. Most eruptions originate in active regions that are, in general, closed magnetic structures rooted in the solar photosphere. Magnetized plasma motions in the solar atmosphere prevent a magnetic structure from attaining a minimum-energy, current-free state. Excess magnetic energy in active regions is manifested by the appearance of electric currents (Leka et al. 1996). Eruptive and noneruptive manifestations, such as coronal mass ejections (CMEs) and confined solar flares, respectively, must be fueled from this reservoir of free magnetic energy that is thought to be released in intermittent episodes of magnetic reconnection.

A popular, early, view of a magnetic energy release event involved a nonpotential pre-event state relaxing into a potential, or nearly potential, post-event state of the magnetic configuration. The excess (nonpotential) magnetic energy was thought to be released during the relaxation. Seminal works on magnetic helicity (Woltjer 1958; Călugăreanu 1961; Berger & Field 1984; Finn & Antonsen 1985; Berger 1985; 1988; Moffatt & Ricca 1992 and others), however, demonstrated that this view is incomplete or even misleading: magnetic helicity relates to the linkage of a magnetic structure (twist, torsion, and writhe), which is globally *invariant* even under resistive processes, such as magnetic reconnection. Helicity is present wherever electric currents are present. Therefore, an isolated helical magnetic structure cannot relax to a potential state unless its magnetic helicity is bodily removed from it. This provides a plausible interpretation for CMEs (Low 1994; Rust 1994a; 1994b), provided that the magnetic helicity in the erupting structures is not transferred to other parts of the solar atmosphere along preexisting or reconnected magnetic field lines. Indeed, eruptive activity seems to be necessary for the Sun where differential rotation and subsurface dynamo continuously generate helicity in the two solar hemispheres (Berger & Ruzmaikin 2000), with a statistical hemispheric segregation exhibited by magnetic structures of opposite senses of helicity (Pevtsov, Canfield, & Metcalf 1995). In confined events the magnetic configuration cannot relax to the potential state but, at best, it may relax to the lowest possible energy state that preserves the pre-event amount of magnetic helicity. This is known to be a constant-alpha, linear force-free (LFF) state (Woltjer 1958; Taylor 1974; 1986). Several works rely on the Woltjer-Taylor theorem, although controversy remains over its applicability to the Sun (Kusano et al. 1994, but also Antiochos & DeVore 1999).

Whether magnetic helicity *per se* is important for solar eruptions is also a subject of debate (e.g. Rust 2003; Rust & LaBonte 2005, but also Phillips, MacNeice, & Antiochos 2005). Regardless, however, knowledge of the magnetic helicity is essential for a complete assessment of the magnetic complexity present in the solar atmosphere. Berger & Field

(1984) and Finn & Antonsen (1985) derived a gauge-invariant definition of magnetic helicity applying to open and multiply connected volumes such as the ones assumed for the solar atmosphere. The resulting *relative* magnetic helicity subtracts the helicity of the reference (potential) field so a nonzero value implies by definition the presence of free magnetic energy in the configuration. The relative magnetic helicity H_m has two equivalent forms in the above works, namely

$$H_m = \int_{\mathcal{V}} (\mathbf{A} \pm \mathbf{A}_p) \cdot (\mathbf{B} \mp \mathbf{B}_p) d\mathcal{V} , \quad (1)$$

where \mathbf{B}_p and \mathbf{A}_p are the potential magnetic field and its generating vector potential, respectively, and \mathbf{B} , \mathbf{A} are the respective quantities of the nonpotential field. The integration refers to the open volume \mathcal{V} that contains the part of the magnetic structure extending above a lower boundary. To derive equation (1), both Berger & Field (1984) and Finn & Antonsen (1985) assumed nonlinear force-free (NLFF) magnetic fields. The force-free approximation is probably necessary for helicity calculations because only in this case one obtains some knowledge of the magnetic field vector and the generating vector potential required to evaluate equation (1).

Equation (1) cannot be evaluated in the active-region atmosphere, however, because the magnetic field vector is unknown above the lower boundary, be it the photosphere or the low chromosphere. Currently, active-region magnetic fields can only be measured in this boundary, so the only way to evaluate the relative magnetic helicity through equation (1) is by force-free (preferably NLFF) field extrapolation into the active-region corona using the measured magnetic fields as the required boundary condition. However, the NLFF extrapolation of observed solar magnetic fields remains an active research area where even the most successful of the existing techniques (Schrijver et al. 2006 and references therein) are too slow to fully exploit the spatial resolution of modern (let alone, future) magnetographs. The NLFF approximation should always be pursued given that the LFF approximation is almost certainly an oversimplification for most active-region fields and it can even be misleading in several cases. Even the NLFF approximation is most likely invalid in the photosphere (Georgoulis & LaBonte 2004), although it may hold in and above the chromosphere (Metcalf et al. [1995]; see, however, Socas-Navarro [2005]).

Even in case equation (1) is evaluated, however, it does not establish a link between the relative magnetic helicity and the magnetic free energy of the studied configuration. In addition, it might be risky to evaluate a volume integral of extrapolated fields at large heights above the boundary because numerical effects might settle in and affect the result. One, therefore, envisions a convenient *surface-integral* representation of the relative magnetic helicity that might alleviate the need for full-fledged three-dimensional extrapolations. To our knowledge, this has been attempted only in the LFF approximation following either the

theoretical analysis of Berger (1985) or the “twist” helicity of Moffatt & Ricca (1992). In the first case (Démoulin et al. 2002; Green et al. 2002), the employed formula for the relative magnetic helicity is

$$H_m = 2\alpha \sum_{l=1}^{n_x} \sum_{m=1}^{n_y} \frac{|b_{u_l, v_m}^2|}{(u_l^2 + v_m^2)^{3/2}} , \quad (2)$$

where α is the unique, representative value of the force-free parameter and b_{u_l, v_m} is the Fourier amplitude of the measured normal magnetic field for the harmonic (u_l, v_m) in a two-dimensional Fourier space with linear dimensions n_x, n_y . Equation (2) is a linearized version of the actual formula of Berger (1985). Linearization helps avoid $|H_m| \rightarrow \infty$ when $|\alpha| \rightarrow (2\pi/L)$, where L is the linear size of the computational domain. Detailed discussions and an extension of Berger’s (1985) analysis will be given in §4.2 and Appendix B. In the second case (Régner, Amari, & Canfield 2005) the magnetic helicity is approximated by the “twist” helicity of a semi-circular, constant-alpha magnetic flux tube, i.e.,

$$H_m = \frac{1}{8}\alpha L\Phi^2 , \quad (3)$$

where L is the characteristic footpoint separation length of the tube and Φ is the magnetic flux carried by the tube. Though useful, equations (2) and (3) also lack a much wanted link between the relative magnetic helicity and the free magnetic energy in the LFF magnetic structure that would enable a complete, self-consistent, description of its energetics. Moreover, it is not clear how to generalize equations (2) and (3) into a NLFF calculation that, as should be always kept in mind, must be the ultimate objective of the calculation.

The above difficulties and lack of information in the calculation of the *total* relative magnetic helicity prompted alternative lines of research. The lower boundary of a closed magnetic structure, where all magnetic field lines are supposed to be rooted, acts as the driver of the evolution in the structure either via boundary flows or via the injection of additional structure through it. Therefore, magnetic helicity can either be transported to and from the structure through this boundary or it can be generated by flows on the boundary¹. Based on these principles, Berger & Field (1984) derived a surface-integral expression for the temporal variation (dH_m/dt) of the relative magnetic helicity in a magnetic configuration. Besides its dependence on magnetic field vectors and vector potentials, as in equation (1), (dH_m/dt) depends on the boundary flows. The advantage of the Berger & Field (1984) expression for (dH_m/dt) is that it does not explicitly require force-free fields. The calculation of (dH_m/dt) has been attempted by numerous authors over the past few years (see, e.g., Nindos 2006;

¹In the Sun, generation of helicity above the photosphere automatically implies the generation of an equal and opposite amount of helicity below the photosphere, to ensure a zero net helicity.

LaBonte, Georgoulis, & Rust 2007, and references therein), although it suffers from the lack of a reference value, namely the *total* relative magnetic helicity. The total relative helicity is a focus of this work, so the formula of Berger & Field (1984) will not be discussed further.

This study is the first of a series of studies that perform a self-consistent calculation of the total magnetic energy and relative magnetic helicity in a closed magnetic configuration. We devise a practical way to calculate magnetic energies and helicities from solar active-region vector magnetograms provided that the observed magnetic configuration is isolated and flux-balanced on the presumed “plane” of the observations. The final expressions for the magnetic energy and helicity are derived in the form of surface, rather than volume, integrals. We always assume that the studied magnetic field configuration is in a force-free equilibrium. In this study, we provide the analytical foundation of a constant-alpha, LFF, energy-helicity calculation. A NLFF generalization of the energy-helicity equations will be the subject of a later study. The LFF analysis of this work relies on the energy-helicity formula of Berger (1988) evaluated via an application and extension of Berger’s (1985) analysis for the magnetic energies and the relative magnetic helicity. Our objective in this work is the derivation of practical LFF energy and helicity equations that can be readily applied to solar vector magnetogram data. The magnetic energy budgets for a constant-alpha magnetic configuration are discussed in §2. The LFF energy-helicity formula is discussed in §3. The relative magnetic helicity is derived both as a volume and as a surface integral in §4. In §5 we apply our LFF analysis to vector magnetograms of two solar active regions and in §6 we summarize and discuss our analysis and results.

2. Gauge-invariant definitions and the magnetic energy equation

2.1. Magnetic field and the vector potential

Assuming planar geometry, consider a magnetic structure \mathbf{B} extending in the half space $z \geq 0$ above a lower boundary \mathcal{S} ($z = 0$). Let an open volume \mathcal{V} of the half space $z \geq 0$ include the structure and extend to infinity with its only boundary being the surface \mathcal{S} . If \mathcal{S} is not a flux (magnetic) surface, i.e. if $\mathbf{B} \cdot \hat{\mathbf{z}}|_{\mathcal{S}} \neq 0$, then the configuration is analogous to a solar magnetic structure rooted in a small (assumed planar) part \mathcal{S} of the photosphere and extending to infinity above \mathcal{S} . Here $\hat{\mathbf{z}}$ is the unit vector along the z -axis of a Cartesian coordinate system with an arbitrary origin on \mathcal{S} . In the absence of plasma, this magnetic configuration can only be the vacuum, current-free magnetic field $\mathbf{B}_{\mathbf{p}}$ if the configuration is isolated (not interacting with other configurations) and flux-balanced on \mathcal{S} . The presence of

plasma dictates a current-carrying magnetic structure \mathbf{B}_c , such that

$$\mathbf{B} = \mathbf{B}_p + \mathbf{B}_c . \quad (4)$$

The divergence-free properties of \mathbf{B} and \mathbf{B}_p together with equation (4) ensure that \mathbf{B}_c is also divergence-free. As a result, we can define generating vector potentials \mathbf{A}_p , \mathbf{A} , and \mathbf{A}_c for \mathbf{B}_p , \mathbf{B} , and \mathbf{B}_c , respectively. By definition,

$$\nabla \times \mathbf{A}_p = \mathbf{B}_p , \quad (5a)$$

$$\nabla \times \mathbf{A} = \mathbf{B} . \quad (5b)$$

In addition, the Coulomb gauge is adopted for both \mathbf{A}_p and \mathbf{A} to provide

$$\nabla \cdot \mathbf{A}_p = 0 , \quad (6a)$$

$$\nabla \cdot \mathbf{A} = 0 . \quad (6b)$$

Since \mathcal{S} is not a flux surface, however, both the definition of \mathbf{B}_p and some topological properties of the field, most notably the ones present in its magnetic helicity integral, are not unique (gauge-invariant) and hence lack a physical meaning (e.g. Dixon et al. 1989; Berger 1999). Berger (1988) addressed the problem by providing gauge conditions for \mathbf{A} and \mathbf{A}_p such that both \mathbf{B}_p and the magnetic helicity can be uniquely defined. These conditions are $\mathbf{A}_p \cdot \hat{\mathbf{n}}|_{\partial\mathcal{V}} = 0$ and $\mathbf{A}_p \times \hat{\mathbf{n}}|_{\partial\mathcal{V}} = \mathbf{A} \times \hat{\mathbf{n}}|_{\partial\mathcal{V}}$ and were formulated for a volume \mathcal{V} bounded by a surface $\partial\mathcal{V}$, where $\hat{\mathbf{n}}$ is the unit vector normal to $\partial\mathcal{V}$ and oriented outward from \mathcal{V} . If \mathcal{V} extends to infinity, Berger (1988) stresses that \mathbf{A}_p and \mathbf{A} *must* additionally vanish at infinity. This restricts the above gauge conditions to the lower boundary \mathcal{S} , so that

$$\mathbf{A}_p \cdot \hat{\mathbf{z}}|_{\mathcal{S}} = 0 , \quad (7a)$$

$$\mathbf{A}_p \times \hat{\mathbf{z}}|_{\mathcal{S}} = \mathbf{A} \times \hat{\mathbf{z}}|_{\mathcal{S}} , \quad (7b)$$

where $\hat{\mathbf{z}} = -\hat{\mathbf{n}}$. From equation (4) and the conditions of equations (5)-(7) we can derive additional conditions for the vector potential \mathbf{A}_c . Writing equation (4) in terms of vector potentials, we obtain $\mathbf{A} = \mathbf{A}_p + \mathbf{A}_c + \nabla\phi$, where ϕ is an arbitrary scalar. Choosing the gauge such that $\nabla\phi = 0$, one obtains

$$\mathbf{A} = \mathbf{A}_p + \mathbf{A}_c , \quad (8)$$

If one now takes the dot and cross products of equation (8) with $\hat{\mathbf{z}}$, then one obtains

$$\mathbf{A}_c \cdot \hat{\mathbf{z}}|_{\mathcal{S}} = \mathbf{A} \cdot \hat{\mathbf{z}}|_{\mathcal{S}} , \quad (9a)$$

$$\mathbf{A}_c \times \hat{\mathbf{z}}|_{\mathcal{S}} = 0 , \quad (9b)$$

where we have used equations (7a) and (7b) to reach equations (9a) and (9b), respectively.

For a volume \mathcal{V} bounded by a surface $\partial\mathcal{V}$, another condition for the uniqueness (gauge-invariance) of \mathbf{B}_p and the magnetic helicity is that \mathbf{B} and \mathbf{B}_p share the same normal component on $\partial\mathcal{V}$, i.e. $\mathbf{B} \cdot \hat{\mathbf{n}}|_{\partial\mathcal{V}} = \mathbf{B}_p \cdot \hat{\mathbf{n}}|_{\partial\mathcal{V}}$. In our case, where \mathcal{V} is only bounded by \mathcal{S} and extends to infinity above \mathcal{S} ($z > 0$), and for \mathbf{A}_p , \mathbf{A} , \mathbf{B}_p , \mathbf{B} vanishing at infinity, the condition refers only to the boundary \mathcal{S} , i.e.

$$\mathbf{B} \cdot \hat{\mathbf{z}}|_{\mathcal{S}} = \mathbf{B}_p \cdot \hat{\mathbf{z}}|_{\mathcal{S}} . \quad (10)$$

It is not necessary to independently pose equation (10), however, as it stems directly from equations (5) and (7b). Take the normal (vertical) components of equation (5a) and (5b) on \mathcal{S} to obtain

$$\nabla_h \cdot (\mathbf{A}_p \times \hat{\mathbf{z}})|_{\mathcal{S}} = \mathbf{B}_p \cdot \hat{\mathbf{z}}|_{\mathcal{S}} \quad , \quad \nabla_h \cdot (\mathbf{A} \times \hat{\mathbf{z}})|_{\mathcal{S}} = \mathbf{B} \cdot \hat{\mathbf{z}}|_{\mathcal{S}} \quad , \quad (11)$$

respectively, where ∇_h denotes differentiation on the horizontal plane, i.e. the boundary \mathcal{S} . Equation (10) immediately follows from combining equations (7b) and (11). In addition, from equations (4) and (10) we obtain $\mathbf{B}_c \cdot \hat{\mathbf{z}}|_{\mathcal{S}} = 0$, so \mathbf{B}_c is a *closed, toroidal* magnetic field on \mathcal{S} . In fact, \mathbf{B}_c is purely toroidal in any cross-section \mathcal{S}' of \mathcal{V} . This has been concluded by Kusano et al. (1994) and Berger (1999) who argued that the net toroidal flux of \mathbf{B}_p and \mathbf{B} should be the same along any cross-section of \mathcal{V} . The potential field \mathbf{B}_p being purely **poloidal**, on the other hand, one expects $\mathbf{B}_p \cdot \mathbf{B}_c = 0$. A construction of \mathbf{B}_p and \mathbf{B}_c by poloidal and toroidal components, respectively, can also be found in Berger (1985).

2.2. Magnetic energy and helicity budgets

From the general equation (4) it is clear that the total magnetic energy $E = [1/(8\pi)] \int_{\mathcal{V}} B^2 d\mathcal{V}$ of a closed magnetic structure is simply the sum of the potential magnetic energy $E_p = [1/(8\pi)] \int_{\mathcal{V}} B_p^2 d\mathcal{V}$ and the nonpotential magnetic energy $E_c = [1/(8\pi)] \int_{\mathcal{V}} B_c^2 d\mathcal{V}$ stored in the configuration in the form of electric currents:

$$E = E_p + E_c . \quad (12)$$

Our objective will be to derive a convenient expression for each of the terms in equation (12). In this section we provide general energy expressions enabled by the gauge invariant definitions of the vector potentials \mathbf{A} , \mathbf{A}_p , and \mathbf{A}_c . Equations for the potential energy E_p can be directly applied to solar magnetic field measurements. Applicable expressions for the total energy E of the magnetic structure are given in the following sections, where the LFF approximation is adopted.

From the definition of A_p , equation (5a), the potential magnetic energy of the configuration is given by

$$E_p = \frac{1}{8\pi} \int_{\partial\mathcal{V}} \mathbf{A}_p \times \mathbf{B}_p \cdot \hat{\mathbf{n}} \, d\sigma \quad , \quad (13)$$

where $d\sigma$ is the surface element on $\partial\mathcal{V}$. To reach equation (13) we have used Gauss's theorem and the current-free condition, $\nabla \times \mathbf{B}_p = 0$. Since \mathbf{A}_p and \mathbf{B}_p , together with \mathbf{A} and \mathbf{B} , all vanish at infinity, however, the above surface integral applies only to the lower boundary \mathcal{S} . The potential energy E_p becomes, therefore,

$$E_p = \frac{1}{8\pi} \int_{\mathcal{S}} \mathbf{B}_p \times \mathbf{A}_p \cdot \hat{\mathbf{z}} \, d\mathcal{S} \quad . \quad (14)$$

Similarly, from the definition of \mathbf{A} , equation (5b), the total magnetic energy of the configuration is given by (see also Berger 1988)

$$E = \frac{1}{8\pi} \int_{\mathcal{S}} \mathbf{B} \times \mathbf{A}_p \cdot \hat{\mathbf{z}} \, d\mathcal{S} + \frac{1}{8\pi} \int_{\mathcal{V}} \mathbf{A} \cdot \nabla \times \mathbf{B} \, d\mathcal{V} \quad . \quad (15)$$

The total energy from equation (15) naturally tends to the potential energy in case the magnetic field vector \mathbf{B} tends to its current-free limit \mathbf{B}_p . Decomposing \mathbf{B} into \mathbf{B}_p and \mathbf{B}_c , one may derive equation (12), where the potential energy is given by equation (14) and $E_c = [1/(8\pi)] \int_{\mathcal{V}} B_c^2 \, d\mathcal{V}$.

In view of the definitions and conditions for \mathbf{A} and \mathbf{A}_p , equations (5)-(7), on the other hand, the relative magnetic helicity of equation (1) can be written as (e.g., Berger 1999)

$$H_m = \int_{\mathcal{V}} \mathbf{A} \cdot \mathbf{B} \, d\mathcal{V} \quad , \quad (16)$$

Equation (14) enables the calculation of the potential energy E_p for a flux-balanced magnetic configuration \mathbf{B} , regardless of whether the magnetic field vector \mathbf{B} is fully known on \mathcal{S} . What is needed is the boundary condition for the vertical field $B_z = \mathbf{B} \cdot \hat{\mathbf{z}}$ on \mathcal{S} , that uniquely determines the potential magnetic field \mathbf{B}_p and its vector potential \mathbf{A}_p on the boundary. In particular, assuming $\mathbf{B}_p = -\nabla\psi$, where ψ is a smooth scalar, $\nabla^2\psi = 0$, Schmidt (1964) showed that

$$\psi(\mathbf{r}, z) = \frac{1}{2\pi} \int \int \frac{B_z(\mathbf{r}') \, dx' \, dy'}{\sqrt{(\mathbf{r} - \mathbf{r}')^2 + z^2}} \quad , \quad (17)$$

where $\mathbf{r} = x\hat{\mathbf{x}} + y\hat{\mathbf{y}}$, $\mathbf{r}' = x'\hat{\mathbf{x}} + y'\hat{\mathbf{y}}$ are vector positions on \mathcal{S} , defined for a given Cartesian coordinate system centered on \mathcal{S} . For the vector potential \mathbf{A}_p one similarly obtains (see also DeVore 2000)

$$\mathbf{A}_p(\mathbf{r}, z) = \nabla \times \hat{\mathbf{z}} \int_z^\infty \psi(\mathbf{r}, z') \, dz' \quad . \quad (18)$$

Although exact, equations (17) and (18) are computationally extensive. Much faster alternatives are provided by means of Fourier transforms. Alissandrakis (1981), in particular, showed that

$$\mathbf{B}_p(\mathbf{r}) = F^{-1}\left(\frac{-iu}{\sqrt{u^2 + v^2}}b_{u,v}\right)\hat{\mathbf{x}} + F^{-1}\left(\frac{-iv}{\sqrt{u^2 + v^2}}b_{u,v}\right)\hat{\mathbf{y}} + B_z\hat{\mathbf{z}} \quad , \quad (19)$$

while Chae (2001) showed that

$$\mathbf{A}_p(\mathbf{r}) = F^{-1}\left(\frac{iv}{u^2 + v^2}b_{u,v}\right)\hat{\mathbf{x}} + F^{-1}\left(\frac{-iu}{u^2 + v^2}b_{u,v}\right)\hat{\mathbf{y}} \quad , \quad (20)$$

where $b_{u,v} = \sum_{l=1}^{L_x} \sum_{m=1}^{L_y} B_{z_{m,l}} \exp[-i(ul + vm)]$ is the Fourier amplitude of B_z , $u = (2\pi l/L_x)$, $v = (2\pi m/L_y)$, L_x , L_y are the linear dimensions of \mathcal{S} , and $F^{-1}(g)$ denotes the inverse Fourier transform of a function g . Albeit much faster, however, equations (19) and (20) assume periodic boundary conditions for \mathbf{B}_p and \mathbf{A}_p which contradicts the assumption of \mathbf{A} and \mathbf{B} vanishing at infinity. This problem is also well known. To mitigate the effects of the periodic boundary conditions assumed when Fourier transforms are used, one typically surrounds the initial flux concentration with a region of zero flux. In our calculations in §5.2 we have applied equations (19) and (20) to zero-buffered magnetograms of solar active regions.

From the above, E_p can be readily calculated for flux-balanced photospheric or chromospheric (not necessarily vector) magnetograms of solar active regions. If a vector magnetogram is available, the vertical field B_z on \mathcal{S} is provided by rotating the measured magnetic field components to the local, heliographic, reference system (Gary & Hagyard 1990). Alternatively, the line-of-sight component can be used instead of B_z provided that the studied active region is located sufficiently close to the center of the solar disk. This requirement typically minimizes the impact of viewing projection effects caused by the curvature of the solar surface.

Unlike the potential magnetic energy E_p , the total magnetic energy E , equation (15), cannot be calculated without additional assumptions or by using line-of-sight magnetograms. This is because \mathbf{A} and $\nabla \times \mathbf{B}$ are generally unknown on and above the (photospheric or chromospheric) boundary \mathcal{S} .

3. The energy-helicity formula in the linear force-free approximation

In the force-free approximation, $(\nabla \times \mathbf{B}) \times \mathbf{B} = 0$, the total magnetic energy E of a structure extending in \mathcal{V} is provided by the magnetic Virial theorem (Molodensky 1974; Aly 1984)

$$E = \frac{1}{4\pi} \int_{\partial\mathcal{V}} \left[\frac{1}{2} B^2 \mathbf{R} - (\mathbf{B} \cdot \mathbf{R}) \mathbf{B} \right] \cdot \hat{\mathbf{n}} d\sigma \quad , \quad (21)$$

where \mathbf{R} is a vector position with arbitrary origin in \mathcal{V} . For planar geometry, \mathcal{V} extending to infinity and being bounded only by \mathcal{S} at $z = 0$, and under the assumption that the magnetic field strength B vanishes with distance more rapidly than $R^{-3/2}$, the Virial theorem reduces to its well-known form

$$E = \frac{1}{4\pi} \int_{\mathcal{S}} \mathbf{r} \cdot \mathbf{B} B_z d\mathcal{S} \ , \quad (22)$$

where $\mathbf{r} = x\hat{\mathbf{x}} + y\hat{\mathbf{y}}$ is a vector position with arbitrary origin on \mathcal{S} . Equation (22) has been applied to solar active regions (Metcalf, Leka, & Mickey 2005; Wheatland & Metcalf 2006) assuming potential or force-free (not necessarily linear) magnetic fields. The explicit dependence of equation (22) on the coordinate system leads to inconsistencies if the employed magnetic field vector is not force-free (for a detailed discussion of problems related to the magnetic Virial theorem see Klimchuk, Canfield, & Rhoads 1992). Although well-known and particularly useful, the Virial theorem does not link the magnetic energy budgets with the relative magnetic helicity in a self-consistent way. For this reason, we will hereafter follow our alternative formulation for the potential magnetic energy (equation (14)) and the total magnetic energy in the LFF approximation. As shown in Figure 8 and explained in §5.2, the Virial theorem and our energy expressions give very similar results.

Implementing the force-free approximation, $\nabla \times \mathbf{B} = \alpha \mathbf{B}$, the total magnetic energy from equation (15) gives

$$E = \frac{1}{8\pi} \int_{\mathcal{S}} \mathbf{B} \times \mathbf{A}_{\mathbf{p}} \cdot \hat{\mathbf{z}} d\mathcal{S} + \frac{1}{8\pi} \int_{\mathcal{V}} \alpha \mathbf{A} \cdot \mathbf{B} d\mathcal{V} \ , \quad (23)$$

and corresponds to the *energy-helicity formula* of Berger (1988). In case of the LFF approximation, where the force-free parameter α is constant in \mathcal{V} , the dependence between E and the relative magnetic helicity H_m becomes explicit. Substituting equation (16) into equation (23) for constant α , we obtain

$$E = \frac{1}{8\pi} \int_{\mathcal{S}} \mathbf{B} \times \mathbf{A}_{\mathbf{p}} \cdot \hat{\mathbf{z}} d\mathcal{S} + \frac{\alpha}{8\pi} H_m \ . \quad (24)$$

Since the relative magnetic helicity depends entirely on the presence of electric currents so that $H_m = 0$ for $\mathbf{B} = \mathbf{B}_{\mathbf{p}}$, the first term in the rhs of equation (24) must correspond to the magnetic energy that does not include the energy stored in electric currents for any *nonzero* α and H_m . This ground-state energy can only be the potential energy E_p , so the energy-helicity formula in the LFF approximation reads

$$E = E_p + \frac{\alpha}{8\pi} H_m \ . \quad (25)$$

A proof of equation (25) is provided in Appendix A.

In a constant-alpha magnetic structure the *sense* (sign) of the relative magnetic helicity H_m is dictated by the *chirality* (sign) of the unique value of the force-free parameter α . Therefore, $\alpha H_m > 0$ by definition in the LFF approximation, where α and H_m are nonzero. If $\alpha H_m = 0$, then both α and H_m are zero by definition. In this case, $E = E_p$ from equation (25). By means of equation (12), moreover, the LFF approximation implies a linear dependence between the free magnetic energy E_c and the relative magnetic helicity H_m , namely,

$$E_c = \frac{\alpha}{8\pi} H_m . \quad (26)$$

The monotonic dependence of E_c on α and H_m can be understood if one considers that both a nonzero relative helicity and a nonzero free energy depend on, and are directly proportional to, the existence of electric currents ($\alpha \neq 0$). Of course, equation (26) is valid only for constant α because the sense of helicity is the same throughout the magnetic structure. For a non-constant α and in case of equal and opposite amounts of helicity being present in the structure, the net relative helicity H_m becomes zero. This would give $E_c = 0$ for $\alpha \neq 0$ in equation (26), which is not true.

Given that the potential energy is readily calculated (equation (14)), it is evident from equation (25) that knowledge of the relative magnetic helicity H_m is sufficient to fully evaluate the LFF energy-helicity formula. However, H_m cannot be evaluated from the general equation (16). This is because the vector potential \mathbf{A} is unknown in \mathcal{V} , although the LFF magnetic field \mathbf{B} can, in principle, be calculated everywhere in \mathcal{V} . In the next section we derive convenient expressions for \mathbf{A} and H_m in the LFF approximation.

4. The relative magnetic helicity in the linear force-free approximation

4.1. Volume-integral representation

It is straightforward to obtain a volume-integral expression for the relative magnetic helicity H_m from the energy-helicity formula, equation (25), using the definitions of the potential and the total magnetic energies:

$$H_m = \frac{1}{\alpha} \int_{\mathcal{V}} (B^2 - B_p^2) d\mathcal{V} . \quad (27)$$

This expression was used by Hagino & Sakurai (2004) who assumed $\mathbf{A} = 0$ on \mathcal{S} . Despite its simplicity, however, equation (27) cannot be directly compared to the general equation (16) because the form of \mathbf{A} is not obvious. To make this conceptual step, we decompose \mathbf{B} in equation (27) into its potential and nonpotential components to find, after some algebra,

that

$$H_m = \frac{1}{\alpha} \int_{\mathcal{V}} \mathbf{B}_c \cdot \mathbf{B} d\mathcal{V} \ , \quad (28)$$

where the condition $\mathbf{B}_p \cdot \mathbf{B}_c = 0$ has been used. Equation (28) is identical to equation (16) for $\mathbf{A} = (1/\alpha)\mathbf{B}_c$, or

$$\mathbf{A} = \frac{1}{\alpha}(\mathbf{B} - \mathbf{B}_p) \ . \quad (29)$$

One may verify that the definition of \mathbf{A} in the LFF approximation, equation (29), complies with all the conditions of equations (5)-(7). Moreover, it is clear that $\mathbf{A}|_{\mathcal{S}} \neq 0$, contrary to what Hagino & Sakurai (2004) assumed. This being said, \mathbf{A} does not have a vertical component on \mathcal{S} because \mathbf{B} and \mathbf{B}_p share the same vertical component on \mathcal{S} , equation (10). Adopting $\mathbf{A} \cdot \hat{\mathbf{z}}|_{\mathcal{S}} = 0$, however, equations (9) will give

$$\mathbf{A}_c \times \hat{\mathbf{z}}|_{\mathcal{S}} = \mathbf{A}_c \cdot \hat{\mathbf{z}}|_{\mathcal{S}} = 0 \ . \quad (30)$$

From equations (30), then, $\mathbf{A}_c|_{\mathcal{S}} = 0$, rather than $\mathbf{A}|_{\mathcal{S}} = 0$. Since $\mathbf{A}_c|_{\mathcal{S}} = 0$, \mathbf{A}_p and \mathbf{A} coincide on \mathcal{S} via equation (8), namely

$$\mathbf{A}|_{\mathcal{S}} = \mathbf{A}_p|_{\mathcal{S}} \ . \quad (31)$$

Of course, equation (31) does not preclude $\nabla \times \mathbf{A}|_{\mathcal{S}} \neq \nabla \times \mathbf{A}_p|_{\mathcal{S}}$. This is because these curls include vertical gradient terms ($\partial/\partial z$) and $\mathbf{A} \neq \mathbf{A}_p$ above \mathcal{S} .

Equation (28) for the relative magnetic helicity satisfies all the requirements of the LFF approximation. Moreover, it is more complete than the equation $H_m = (1/\alpha) \int_{\mathcal{V}} B^2 d\mathcal{V}$ of Pevtsov, Canfield, & Metcalf (1995). Clearly, from the above expression $\lim_{\alpha \rightarrow 0} |H_m| = E_p \lim_{\alpha \rightarrow 0} (1/|\alpha|)$, which tends to infinity while it should tend to zero. Given that \mathbf{B} in equation (28) corresponds to an LFF magnetic field, the integrand $\mathbf{B}_c \cdot \mathbf{B} = B^2 - \mathbf{B} \cdot \mathbf{B}_p$ is known at any location in \mathcal{V} if B_z is known and flux-balanced on \mathcal{S} . Therefore, the total relative magnetic helicity of a closed and flux-balanced magnetic structure with constant α in \mathcal{V} can be calculated using equation (28). By extension, equation (28) can be used to calculate the total relative magnetic helicity of an isolated solar active region for which the constant-alpha approximation is assumed valid and for which flux-balanced photospheric or chromospheric vector magnetic field measurements exist. A representative, unique value of the force-free parameter α can be calculated by an array of techniques (Leka & Skumanich 1999; Leka 1999) with an alternative technique described in §5.1.

In theory, one may estimate the relative magnetic helicity from the volume integral of equation (28). In practice, however, it would be both risky and computationally extensive to apply equation (28) to extrapolations of actual solar magnetic configurations. This is because

(i) despite the treatment of periodic effects on the horizontal plane, Fourier transforms in the LFF approximation can still cause periodic effects in the vertical direction and at large heights above the photosphere (i.e., Alissandrakis 1981; Gary 1989), and (ii) one does not know *a priori* the height above the photosphere where integration should stop. There are some partial remedies for both of the above problems: the use of a much larger computation volume than that required to contain the magnetic structure may limit periodic effects within \mathcal{V} , while the maximum integration height can be either equal to the linear size of the surface \mathcal{S} or determined by the contribution to the relative magnetic helicity H_m . If integration above a certain height makes insignificant contributions to H_m then integration stops at this height. In any case, calculating H_m from equation (28) is a very time-consuming task. For this reason, we derive in the next section a first-principles *surface* integral for H_m in the LFF approximation.

4.2. Surface-integral representation based on Fourier transforms

Regardless of the force-free approximation, the total magnetic energy E of a closed magnetic structure extending into \mathcal{V} and rooted in \mathcal{S} consists of the potential magnetic energy E_p of the structure and the nonpotential (free) magnetic energy E_c due to electric currents (equation (12)). Expressing E_c in terms of E_p , one may write

$$E = (1 + f)E_p \quad , \quad (32)$$

where $E_c = fE_p$ and f is generally a positive and dimensionless variable. The constant-alpha approximation readily provides a condition for f , namely $\lim_{\alpha \rightarrow 0} f = 0$. In addition, f must be a function of α and increasing $|\alpha|$ should increase f monotonically giving rise to a symmetric profile of $f(\alpha)$ with respect to $\alpha = 0$, i.e. $f(|\alpha|) = f(-|\alpha|)$. The form of f can be derived analytically in the LFF approximation if one uses the formulation of Berger (1985). The details of the derivation are given in Appendix B. Here we provide two expressions for the variable f . The first is the exact analytical formula, while the second is a linearized, with respect to α^2 , version f_l of it, useful to keep the free energy and relative helicity finite when $|\alpha|d \rightarrow (2\pi/L)$, where d is the elementary size on the boundary \mathcal{S} and L is the linear size of the magnetic structure on \mathcal{S} . For an observed magnetogram, d corresponds to the linear size of a pixel expressed in physical units. In particular,

$$f = \mathcal{F} \quad , \quad \text{and} \quad f_l = \mathcal{F}_l d^2 \alpha^2 \quad , \quad (33)$$

where

$$\mathcal{F} = \frac{\sum_{l=1}^{n_x} \sum_{m=1}^{n_y} |b_{u_l, v_m}^2| \frac{(u_l^2 + v_m^2)^{1/2} - (u_l^2 + v_m^2 - \alpha^2 d^2)^{1/2}}{(u_l^2 + v_m^2)^{1/2} (u_l^2 + v_m^2 - \alpha^2 d^2)^{1/2}}}{\sum_{l=1}^{n_x} \sum_{m=1}^{n_y} \frac{|b_{u_l, v_m}^2|}{(u_l^2 + v_m^2)^{1/2}}} \quad , \quad (34a)$$

and

$$\mathcal{F}_l = \frac{1}{2} \frac{\sum_{l=1}^{n_x} \sum_{m=1}^{n_y} \frac{|b_{u_l, v_m}^2|}{(u_l^2 + v_m^2)^{3/2}}}{\sum_{l=1}^{n_x} \sum_{m=1}^{n_y} \frac{|b_{u_l, v_m}^2|}{(u_l^2 + v_m^2)^{1/2}}} , \quad (34b)$$

respectively. In equations (34), b_{u_l, v_m} is the Fourier amplitude of the vertical magnetic field B_z for the harmonic (u_l, v_m) in a Fourier space with dimensions n_x, n_y . The linearization f_l implies a minimum value for f that results in the estimation of a minimum free magnetic energy E_c and relative magnetic helicity $|H_m|$ in the LFF approximation. The underestimation of E_c and H_m is negligible for small $|\alpha|$ and increases as α increases (see §4.3 below and Figure 1). This effect is explained in detail in Appendix B and has been realized by several previous works when the linearized relative helicity expression of equation (2) was derived (Green et al. 2002; Démoulin et al. 2002; Démoulin 2006). The infinite energy and helicity for $(|\alpha|/d) \rightarrow (2\pi/L)$ is a well-known problem of the LFF magnetic fields that are not fully described by the boundary condition on \mathcal{S} in this case (e.g., Alissandrakis 1981).

The quadratic dependence of f on α in both the exact and the linearized case guarantees a symmetric profile of $f(\alpha)$ and a vanishing f for $\alpha \rightarrow 0$. This dependence has also been demonstrated graphically by Sakurai (1981) in analytical force-free fields.

From equations (32) and (33) we can now parameterize all terms of the energy-helicity formula (equation (25)) with respect to one of these terms. As the free parameter we choose the potential magnetic energy E_p for which the general expression of equation (14) exists. Then, the exact and the linearized surface-integral expressions for the total magnetic energy in a constant-alpha magnetic structure read

$$E = (1 + \mathcal{F})E_p , \quad (35a)$$

and

$$E = (1 + \mathcal{F}_l d^2 \alpha^2)E_p , \quad (35b)$$

respectively. For the free magnetic energy we obtain

$$E_c = \mathcal{F}E_p , \quad (36a)$$

and

$$E_c = \mathcal{F}_l d^2 \alpha^2 E_p , \quad (36b)$$

respectively, while for the relative magnetic helicity we find

$$H_m = \frac{8\pi}{\alpha} \mathcal{F}E_p , \quad (37a)$$

and

$$H_m = 8\pi \mathcal{F}_l d^2 \alpha E_p , \quad (37b)$$

respectively. Notice that the exact formula for the relative helicity, equation (37a), still yields $|H_m| \rightarrow 0$ for $|\alpha| \rightarrow 0$ because $\mathcal{F} \propto \alpha^2$ tends to zero faster than α . Equation (37b) gives values that are a factor of four smaller than those of the linearized relative helicity of Démoulin et al. (2002) and Green et al. (2002) (equation (2)). This can be seen from equations (37b) and (B3), and by setting $d = 1/(2\pi)$, which corresponds to Berger’s (1985) unit length assuming a computational box with linear size L equal to unity. Part of the discrepancy has been corrected by Démoulin (2006) who admits that the original expression of equation (2) was a factor of two too high. In Appendix B we show that the linearization introduces an additional (1/2)-factor in equation (34b).

Concluding, equations (35) - (37) offer convenient surface-integral representations of the relative magnetic helicity, as well as of the total and the nonpotential magnetic energies in the LFF approximation. Equations (14) and (35)-(37) will be evaluated in §§4.3 and 5 for semi-analytical and observed magnetic configurations, respectively.

From equations (35) - (37) we can calculate the uncertainties δE , δE_c , and δH_m of the total magnetic energy, the free magnetic energy, and the total magnetic helicity, respectively. Uncertainties of the potential energy, equation (14), stem from the uncertainties δB_z of the normal (vertical) magnetic field component B_z . Although the values of δB_z are generally known for a given magnetogram, it is difficult to propagate them into the potential energy because of the extrapolations required to infer the potential magnetic field and its vector potential. In our case the extrapolations are performed using Fast Fourier transforms. For this reason we will ignore the uncertainties δE_p of the potential energy, although we expect that these uncertainties should not be very significant, given that the vertical magnetic field component is the least uncertain measured component of the magnetic field vector, especially for active regions located close to the center of the solar disk. For the same reason we will also ignore the uncertainties $\delta \mathcal{F}_l$ of \mathcal{F}_l . Excluding δE_p and $\delta \mathcal{F}_l$, the only source of uncertainties is the uncertainties $\delta \alpha$ in the inference of the force-free parameter α . These uncertainties give rise to a nonzero $\delta \mathcal{F}$ in the value of \mathcal{F} (equation (34a)). From equations (35) - (37), then, we obtain the following uncertainty expressions:

For the exact and linearized total magnetic energy,

$$\frac{\delta E}{E} = \frac{E_c}{E} \frac{\delta \mathcal{F}}{\mathcal{F}} \ , \quad (38a)$$

and

$$\frac{\delta E}{E} = 2 \frac{E_c}{E} \frac{\delta \alpha}{|\alpha|} \ , \quad (38b)$$

respectively. For the free magnetic energy,

$$\frac{\delta E_c}{E_c} = \frac{\delta \mathcal{F}}{\mathcal{F}} \ , \quad (39a)$$

and

$$\frac{\delta E_c}{E_c} = 2 \frac{\delta \alpha}{|\alpha|} , \quad (39b)$$

respectively. For the relative magnetic helicity,

$$\frac{\delta H_m}{|H_m|} \leq \sqrt{\left(\frac{\delta \alpha}{\alpha}\right)^2 + \left(\frac{\delta \mathcal{F}}{\mathcal{F}}\right)^2} , \quad (40a)$$

and

$$\frac{\delta H_m}{|H_m|} = \frac{\delta \alpha}{|\alpha|} , \quad (40b)$$

respectively. The “ \leq ” symbol in equation (40a) is due to the fact that \mathcal{F} and α are interrelated. Given that it is also difficult to propagate the uncertainties of $|\alpha|$ into $\delta \mathcal{F}$, we will hereafter use the linearized expressions of the uncertainties, equations (38b) - (40b).

4.3. Comparison between the volume- and the surface-integral expressions for the relative magnetic helicity

At this point we have derived two types of expressions for the relative magnetic helicity in the LFF approximation, namely the volume integral of equation (28) and the surface integrals of equations (37). To ensure consistency, these expressions must provide nearly identical results for small values $|\alpha|$ of the force-free parameter, while the linearized expression of equation (37b) must provide a lower limit of the relative magnetic helicity as $|\alpha|$ increases. To avoid errors due to observational uncertainties and to make a safer evaluation of the volume integral of equation (28) we use semi-analytical models of magnetic structures, rather than observed solar magnetograms. For a simple representation of the twist present in the magnetic configurations we use dipolar magnetic field models. For a given dipole with footpoint separation L_{sep} , we define the dimensionless quantity $N = \alpha L_{sep}$. This quantity is generally a dimensionless measure of α . In the particular case of field lines winding about an axis (not necessarily assumed here), N is a measure of the total end-to-end number of turns of the dipole. Our dipoles are characterized according to their N -values. We first create the analytical distribution for the vertical magnetic field B_z normal to the horizontal plane \mathcal{S} and then we apply LFF extrapolations in the volume \mathcal{V} using the same B_z -distribution as boundary condition and assuming different α -values stemming from different N -values in each extrapolation. Extrapolations are performed using the Fast Fourier transform method of Alissandrakis (1981). For this test we use positive α -values which results in right-handed helicities. Using equal and opposite α -values would only change the sense of twist and hence the sign, but not the magnitude, of the calculated magnetic helicity. The magnetic energy budgets, equations (35) - (36), are insensitive to the sign of α .

Our model dipoles have a fixed footpoint separation length $L_{sep} = 100$ (in arbitrary units) and are embedded in a boundary plane \mathcal{S} with linear dimensions $L_x = L_y = 200$, assuming an elementary length $d = 1$ as the unit length. The separation length L_{sep} represents the distance between the positive- and the negative-polarity centers of the dipole on \mathcal{S} . We use an array of N -values, where $N \in [0.02, 2]$, each of which determines a different $\alpha = (N/L_{sep})$. To make sure that equations (35) - (37) do not depend on the details of a particular model, we use three different models of B_z on \mathcal{S} . For each model, the two polarity centers are placed at vector positions \mathbf{r}_1 and \mathbf{r}_2 , respectively, on \mathcal{S} , such that $|\mathbf{r}_1 - \mathbf{r}_2| = L_{sep}$. The number of harmonics used for the Fourier-transform calculation of \mathcal{F} and \mathcal{F}_l , equations (37a) and (37b), respectively, is kept fixed in all cases and is equal to $n_x = n_y = 256$. We use the following models:

- (1) A Gold-Hoyle dipole solution (Gold & Hoyle 1960), i.e.,

$$B_z(\mathbf{r}) = B_0 \left[\frac{1}{1 + q(\mathbf{r} - \mathbf{r}_1)^2} - \frac{1}{1 + q(\mathbf{r} - \mathbf{r}_2)^2} \right] , \quad (41)$$

where \mathbf{r} is the vector position of a given location on \mathcal{S} and B_0, q are positive constants. In this test we have used a fixed $B_0 = 10^3$ and an array of q -values, $q \in [0.5, 10]$. Each q -value has been applied to the full array of N -values.

- (2) A solenoidal dipole solution (Sakurai & Uchida 1977), i.e.,

$$B_z(\mathbf{r}) = \frac{B_0}{16\pi} (16 + \pi^2 \bar{L}_{sep}^2)^{3/2} \sum_{i=1}^2 \left\{ \frac{s_i}{\sqrt{16(1 + \bar{\rho}_i)^2 + \pi^2 \bar{L}_{sep}^2}} [I_1(k_i) + \frac{16(1 - \bar{\rho}_i^2) - \pi^2 \bar{L}_{sep}^2}{16(1 - \bar{\rho}_i)^2 + \pi^2 \bar{L}_{sep}^2} I_2(k_i)] \right\} , \quad (42)$$

where $s_1 = 1, s_2 = -1, q$ is a positive constant, $\bar{\rho}_i = (\rho_i/q); i \equiv \{1, 2\}$, are the normalized, with respect to q , distances of a location \mathbf{r} on \mathcal{S} from \mathbf{r}_1 and \mathbf{r}_2 ($\rho_i = |\mathbf{r} - \mathbf{r}_i|; i \equiv \{1, 2\}$), $\bar{L}_{sep} = L_{sep}/q$ is the normalized, with respect to q , separation length, $k_i^2 = 64\bar{\rho}_i/[16(1 + \bar{\rho}_i)^2 + \pi^2 \bar{L}_{sep}^2]$, and $I_1(k_i), I_2(k_i)$ are the complete elliptic integrals of the first and second kind, respectively, i.e.,

$$I_1(k_i) = \int_0^{\pi/2} \frac{d\theta}{\sqrt{1 - k_i^2 \sin^2 \theta}} \quad \text{and} \quad I_2(k_i) = \int_0^{\pi/2} \sqrt{1 - k_i^2 \sin^2 \theta} d\theta . \quad (43)$$

Here we have used a fixed $B_0 = 10^3$ and an array of q -values, $q \in [0.02, 0.3]$, each value of which has been applied to the full array of N -values.

- (3) A submerged poles dipole solution (Longcope 2005 and references therein), i.e.,

$$B_z(\mathbf{r}) = B_0 q \left\{ \frac{1}{[(\mathbf{r} - \mathbf{r}_1)^2 + q^2]^{3/2}} - \frac{1}{[(\mathbf{r} - \mathbf{r}_2)^2 + q^2]^{3/2}} \right\} , \quad (44)$$

where B_0 and q are positive constants. The constant q , in particular, represents the depth below \mathcal{S} in which the two magnetic monopoles are placed. The depth of each monopole can, in principle, be different than that of the other(s), but here we use a fixed depth, as well as a fixed magnetic field strength B_0 for each monopole, to create a flux-balanced magnetic configuration on \mathcal{S} . Here we use $B_0 = 10^3$ and an array of depths q , $q \in [0.5, 10]$, each value of which has been applied to the full array of N -values.

Comparing the volume-integral expression, equation (28), with the surface-integral expressions, equations (37), for the relative magnetic helicity H_m gives the expected results for all q - and N -values. Three of these results, one for each model, are given in Figure 1a. The q -values for each model in Figure 1a were selected with the sole purpose of giving rise to well-separated helicity values, for convenience in the visual comparison. These selections are $q = 0.6$, 0.2 , and 10 for the Gold-Hoyle (GH), the Sakurai-Uchida (SU) and the submerged-poles (SP) model, respectively. Figure 1a gives rise to the following conclusions:

- (1) All helicity expressions give very similar results for a given model, which suggests that the LFF equations (35) - (37) are model-independent.
- (2) For $N = \alpha L_{sep} \rightarrow 0$, all expressions give $H_m \rightarrow 0$. Therefore, H_m from equations (28) and (37) corresponds to the gauge-invariant relative magnetic helicity discussed in §§4.1 and 4.2. As α increases for a fixed L_{sep} , Figure 1a shows the quadratic increase of the magnetic helicity in the dipoles, for a fixed boundary condition B_z on \mathcal{S} .
- (3) Clearly, all expressions for H_m give nearly identical results for small α . As α increases, the linearized surface-integral expression (equation (37b); dotted curves) consistently provides a lower H_m (the exact surface-integral expression of equation (40a) is represented by solid curves and rectangles), as expected. The volume-integral expression for H_m (equation (28); dashed curves and triangles) gives slightly higher values than both surface-integral expressions.

Tests with $N > 2$ (not shown in Figure 1) reveal that the volume-integral H_m increases exponentially after some maximum N -value, while the surface-integral expressions continue to increase quadratically². This maximum N -value is model-dependent and, in case of the SP model, it changes even with varying model parameters. This inability to predict the

²Of course, at the vicinity of $|\alpha|d \simeq (2\pi/L)$, which in our parameter selection corresponds to $N = \pi$, the exact surface-integral H_m increases abruptly to become infinite for $|\alpha|d = (2\pi/L)$

behavior of the volume-integral H_m for large N , combined with spurious results of the Fourier-transform extrapolations in these cases, enhances one’s impression that the volume-integral helicity is less reliable than the surface-integral expressions and that, among other problems, it is susceptible to artifacts incurred by Fourier-transform extrapolations at large heights above the boundary \mathcal{S} .

Figure 1b shows the underestimation factor caused by the use of the linearized surface-integral expression of equation (37b) for the three cases depicted in Figure 1a. In particular, the dashed curves show the ratio between the volume-integral and the linearized surface-integral helicities, while the solid curves show the ratio between the exact surface-integral and the linearized surface-integral helicities. Evidently, the underestimation factor is nearly model-independent when the two surface-integral expressions are compared, while the situation is less predictable when the volume-integral and the linearized surface-integral expressions are compared. From the comparison between the surface-integral helicity expressions, one sees that, even for large N -values, underestimation does not exceed a factor of ~ 1.85 . For dipolar solar active regions for which the LFF approximation is assumed and with typical values of $\alpha \sim 10^{-2} Mm^{-1}$ and $L_{sep} \sim 100 Mm$, we obtain $N \sim 1$. The expected underestimation factor for this case is $\lesssim 1.1$, which is very modest compared to the errors expected from other assumptions, and especially the use of the constant-alpha approximation itself.

In summary, the results shown in Figure 1 demonstrate that the surface-integral expressions of equations (37) lead to reliable estimates of the total relative magnetic helicity in a constant-alpha magnetic structure. By extension, the surface integrals of equations (35) and (36) provide reliable estimates of the total magnetic energy and the free magnetic energy, respectively, in the structure.

5. Application to observed solar active region magnetic fields

5.1. Data selection and determination of basic parameters

In this section we apply the results of the previous analysis to vector magnetograms of solar active regions. In particular, we calculate the LFF magnetic energy and helicity budgets (equations (14) and (35) - (37)) using photospheric vector magnetogram data obtained by the Imaging Vector Magnetogram (IVM; Mickey et al. 1996; LaBonte, Mickey, & Leka 1999) of the University of Hawaii’s Mees Solar Observatory. IVM’s photospheric magnetog-

raphy³ consists of recording the complete Stokes vector at each of 30 spectral points through the Fe I 6302.5 Å photospheric spectral line. The line-of-sight magnetic field components are obtained via the inversion code of Landolfi & degl’Innocenti (1982) that includes LTE radiative transfer, magneto-optic effects, and the filling factor of the unresolved flux tubes. Our equations are applicable to the heliographic magnetic field components on the heliographic plane. The required coordinate transformation has been carried out following the analysis of Gary & Hagyard (1990).

To test our derivations for energy and helicity, we study two solar active regions (ARs): a small, short-lived emerging flux region (NOAA AR 8844) and a persistent, large, and complex AR that exhibited significant eruptive activity (NOAA AR 9165). For both ARs, the IVM recorded a series of vector magnetograms over a period of a few hours that can be used to follow the temporal evolution of the energy and helicity budgets in the regions.

Before applying any analysis that employs the transverse field of a vector magnetogram, one must first resolve the intrinsic azimuthal ambiguity of 180° in the orientation of the transverse magnetic field component. Azimuth disambiguation of the employed IVM magnetograms was performed by means of the nonpotential magnetic field calculation (NPFC) method of Georgoulis (2005a) - see also Metcalf et al. (2006) for a comparative evaluation of the method with respect to other disambiguation methods. Figures 2a and 2b depict two disambiguated vector magnetograms of NOAA ARs 8844 and 9165, respectively. Only part of the IVM field of view is shown in both images, to exemplify the magnetic structure of the two ARs. Shown are the heliographic magnetic field components on the heliographic plane. The relative isolation of the two ARs on the solar disk at the time of the IVM observations (2000 January 25 and September 15 for ARs 8844 and 9165, respectively), as well as the ARs’ very different records of eruptive activity prompted us to use these data in this first test of our LFF energy / helicity calculations.

The timeseries of the magnetic flux Φ during the IVM observing interval for both ARs are shown in Figure 3. For both cases, we notice that the IVM field of view encloses fairly well-balanced magnetic flux distributions. NOAA AR 8844 is more flux-balanced than NOAA AR 9165, with an imbalance always kept below 5%. The maximum imbalance of NOAA AR 9165 is around 10%. Our derivations require flux-balanced magnetic structures and the above slight imbalances are not expected to significantly impact our results. The first noticeable difference between the two ARs is in their respective amounts of magnetic flux: on average, the magnetic flux in NOAA AR 9165 ($\Phi \sim 17.1 \times 10^{21} Mx$) is a factor of ~ 3.4

³Recently, the IVM focused on the chromospheric magnetically sensitive line Na I (5896 Å). These observations have started providing *chromospheric* vector magnetograms of solar active regions.

larger than the flux in NOAA AR 8844 ($\Phi \sim 5.1 \times 10^{21} \text{ Mx}$). One might also notice a very slight increasing trend in the evolution of Φ in NOAA AR 8844 (from $\sim 4.9 \times 10^{21} \text{ Mx}$ to $\sim 5.3 \times 10^{21} \text{ Mx}$) within the 2 *hr* of the IVM observations, implying that the magnetic structure is growing. This is typical of emerging flux regions.

After disambiguation, we need to calculate a unique force-free parameter α for each magnetogram. To do so, we calculate the slope in the scatter plot between the vertical curl $(\nabla \times \mathbf{B})_z$ of the magnetic field \mathbf{B} and the vertical field B_z for strong-field locations of the magnetograms. By strong-field locations we mean locations with magnetic field components exceeding the 1σ threshold, where we have taken 1σ to correspond to a vertical magnetic field of 100 *G* and a horizontal magnetic field of 200 *G*, typical of the IVM. Because the LFF approximation is a gross simplification of the photospheric active-region magnetic fields, however, the uncertainty in the value of the slope is often larger than the slope itself due to the substantial scatter in the pairs of $[(\nabla \times \mathbf{B})_z, B_z]$ -values. To restrict the uncertainty in the calculation of α we have developed the following procedure: we obtain several α -values from the slope of the scatter plot, each calculated using a different significance threshold, as shown in Figure 4. Let α_k be the value of α for a given significance threshold $\sigma_k = k\sigma$; $k \geq 1$ and Φ_k be the respective unsigned magnetic flux used in the calculation. Then, the adopted unique value of α and its uncertainty $\delta\alpha$ are obtained by the flux-weighted averages

$$\alpha = \frac{\sum_k \alpha_k \Phi_k}{\sum_k \Phi_k} \quad \text{and} \quad \delta\alpha = \frac{\sum_k |\alpha - \alpha_k| \Phi_k}{\sum_k \Phi_k}, \quad (45)$$

respectively. An example of this calculation is shown in Figure 4. The flux-weighted average α is indicated by the solid line and the surrounding shaded area indicates the extent of its uncertainty $\delta\alpha$. The above process provides a maximum-likelihood α -value with a reasonable uncertainty and is repeated for every vector magnetogram of the timeseries to obtain the respective timeseries for α . Using other methods to calculate α (see, e.g., Leka & Skumanich 1999 and Leka 1999) we verified that the timeseries of α obtained by equations (45) are more smooth (less spiky) and with smaller uncertainties for each α -value, than the α -timeseries stemming from the other methods.

5.2. Magnetic energy and helicity calculations

The timeseries of the force-free parameter α for both tested ARs are shown in Figure 5. As we discussed in §5.1, the different α -values are generally consistent with each other, giving rise to fairly well-defined averages in both cases. The overall twist for NOAA AR 8844 is right-handed ($\alpha > 0$), while for NOAA AR 9165 it is left-handed ($\alpha < 0$). For the latter AR, in particular, α appears to decrease, in absolute value, in the course of time. Coincidentally,

the average absolute values $|\bar{\alpha}|$ of α for both ARs are almost identical ($\bar{\alpha} = 0.023 \pm 0.06 \text{ Mm}^{-1}$ and $\bar{\alpha} = -0.024 \pm 0.06 \text{ Mm}^{-1}$ for NOAA ARs 8844 and 9165, respectively). We note in passing that the value of $\bar{\alpha}$ for NOAA AR 8844 is in excellent agreement with the value of 0.022 Mm^{-1} , calculated by Pariat et al. (2004). The latter α -value was inferred by combining the best LFF match of the active-region corona using simultaneous EUV images from TRACE with a best LFF fit of the observed horizontal magnetic field. The magnetic field vector in Pariat et al. (2004) was acquired by the high-resolution vector magnetograph onboard the balloon-borne Flare Genesis Experiment (FGE; Bernasconi et al. 2001).

Although the two studied ARs happen to have almost the same α -values, albeit with different signs, the much larger magnetic flux carried by the eruptive NOAA AR 9165 is expected to lead to much larger energy / helicity budgets than the respective budgets of the noneruptive NOAA AR 8844. The relative magnetic helicity and the respective magnetic energies for ARs 8844 and 9165 are plotted in Figures 6 and 7, respectively. There we show both the linearized (equations (35b)-(37b); red curves) and the exact (equations (35a)-(37a); blue curves) surface-integral expressions for energy and helicity. Before discussing and comparing individual values, we note that the linearized expressions generally provide slightly lower magnitudes of energy and helicity. This is clearly the case for NOAA AR 8844 (Figure 6), while in cases where the linearized values are larger than the exact values for NOAA AR 9165 (Figure 7), the difference is within error bars. That the linearized expressions provide lower limits of energy and helicity was concluded from the analysis in Appendix B and verified using semi-analytical models in §4.3. In both cases of observed ARs, moreover, the timeseries of the exact values appear more spiky than the respective timeseries of the linearized values. Given that the linearized expressions lead to a smoother temporal evolution with slightly lower values than the exact expressions, equations (35b) - (37b) for the linearized energy and helicity budgets appear preferable compared to the exact expressions of equations (35a) - (37a). Besides being more convenient and well-behaved, the linearized expressions also have readily derivable uncertainties (equations (38b) - (40b)) based on the uncertainties $\delta\alpha$ of α . This being said, one notices the close correspondence of the α -value timeseries of Figures 5 with the timeseries of the linearized helicity of Figures 6 and 7. Clearly, the success of the LFF energy/helicity estimations depends on the reliability of the inference of α . This is a key feature that one should keep when trying to generalize the LFF energy/helicity formulas into NLFF ones, valid for a variable α within the field of view.

The average energy/helicity values from Figures 6 and 7 are summarized and compared in Tables 1 and 2. Table 1 shows the comparison between average magnetic fluxes, α -values, and helicities, while Table 2 focuses on the comparison between the various average energy budgets from the two ARs. It is quite useful that the average α -values are nearly identical

for the two ARs. We then notice that the eruptive NOAA AR 9165, with a factor of ~ 3.4 larger magnetic flux than the noneruptive NOAA AR 8844, also has a potential and a total magnetic energy that are similarly (by a factor of $\sim 3.2-3.5$) larger than those of NOAA AR 8844. The average relative magnetic helicity and free magnetic energy of the eruptive AR, however, are $\sim 7.6-8.9$ times larger than those of the noneruptive AR. Notably, the linearized expressions, that result in lower values and uncertainties, consistently give a higher factor of difference in both energy and helicity. The much wider difference between the free energy and the relative helicity between the two ARs suggests that a viable criterion (safer than simply evaluating the magnetic flux) for distinguishing between eruptive and noneruptive ARs may be the amount of free magnetic energy and helicity. This study should, of course, be applied to a large number of eruptive and noneruptive ARs for the results to obtain statistical significance. Moreover, if this treatment is generalized to the NLFF, rather than the LFF, approximation, it will be much more physically meaningful given the expected conditions in the low solar atmosphere. Forced photospheric fields (see, e.g., Georgoulis & LaBonte (2004)) should still lead to discrepancies stemming from the application of the force-free approximation. Another notable fact from Table 2 is the fractional free magnetic energy (\bar{E}_c/\bar{E}), normalized by the total magnetic energy. For the noneruptive NOAA AR 8844, the free energy is $\sim 4.7\%$ - 6% of the total magnetic energy. For the eruptive NOAA AR 9165, the free energy corresponds to $\sim 12.3\%$ - 13.1% of the total energy, which is a factor of $\sim 2.2 - 2.6$ higher.

Notice the the above ratios of the free to the total energy are substantially lower than those calculated by Metcalf, Leka, & Mickey (2005), for NOAA AR 10486, on 2003 October 29. Using the Virial theorem and implicitly assuming NLFF magnetic fields, these authors found that the free energy ranged from $\sim 44\%$ (a few hours before a major X10 flare) to $\sim 75 - 80\%$ (in the course of, and shortly after, the flare), of the total energy. These ratios appear extraordinarily high, at least in view of eruption models that predict the eruption onset when the free energy exceeds $10 - 15\%$ of the total energy (see, for example, DeVore & Antiochos 2005). Of course, NOAA AR 10486 was an extraordinary AR, which might account for its unusual behavior.

Despite the large difference of energy and helicity budgets between the two ARs, notice that significant magnetic helicity is present even in the noneruptive NOAA AR 8844. Indeed, the average relative helicity of the AR is $\bar{H}_m \simeq (1.5 \pm 0.4) \times 10^{42} Mx^2$, with the helicity budget of a typical CME estimated at $\sim 2 \times 10^{42} Mx^2$ (DeVore 2000). With a minor helicity increase, therefore, the AR should be capable of producing a typical CME before relaxing to the potential state. Interestingly, a faint halo CME occurred above the AR on 2000 January 26 at $\sim 12:00$ UT and the AR started to decay less than $24 hr$ later, on 2000 January 27 (Schmieder et al. 2004). As the AR was still growing during the IVM observations, it is

likely that its magnetic helicity was further increased by January 26. No significant flaring activity was associated to the CME.

NOAA AR 9165, on the other hand, gave an eruptive M2 flare a few hours before the IVM observations on 2000 September 15, as well as two even stronger eruptive flares (M5.9 and M3.3) on the next day. Its relative magnetic helicity, $\sim (-13 \pm 4) \times 10^{42} Mx^2$ was enough to launch nearly seven typical CMEs. Perhaps not surprisingly, the AR survived for several more days and could clearly be followed until it crossed the western solar limb.

Back in our analysis, the compromise brought by the LFF approximation is reflected on the uncertainties accompanying the estimations of the free magnetic energy in both ARs. Obviously, the free magnetic energy is a crucial parameter in assessing the eruptive potential of a given AR (see, e.g., Metcalf, Leka, & Mickey 2005). With average linearized free energies of $(0.15 \pm 0.1) \times 10^{32} \text{ erg}$ and $(1.33 \pm 0.6) \times 10^{32} \text{ erg}$ for NOAA ARs 8844 and 9165, respectively, the lowest uncertainties are estimated at $\sim 67\%$ and $\sim 45\%$, respectively. A generalization allowing NLFF fields will hopefully restrict these uncertainties.

Finally, in Figure 8 we compare our estimated potential and total magnetic energies, equations (14) and (35) - (36), with those obtained by the calculation of the Virial theorem, equation (22), for both ARs. To implement the Virial theorem, we perform a current-free and a LFF extrapolation of each IVM magnetogram, the latter using the inferred maximum-likelihood α -value for this magnetogram. Estimates of the Virial theorem are represented by dashed curves and triangles. Solid curves and rectangles refer to the linearized expressions, while dotted curves refer to the exact expressions. For a convenient comparison, the scaling for the potential energy (blue curves) is different than the scaling for the total energy (red curves). From the plots in Figure 8, we first notice that our potential-energy expression, equation (14), gives almost identical results with the Virial theorem for both ARs. The average fractional differences $|E_p - E_{p(\text{virial})}| / (E_p + E_{p(\text{virial})})$ are $\sim 0.7\%$ and $\sim 0.2\%$ for ARs 8844 and 9165, respectively. The difference is larger for the total energies. On average, the fractional difference is $\sim 1.6\%$ ($\sim 1.1\%$) for the linearized (exact) expressions in NOAA AR 8844. For NOAA AR 9165, the average fractional difference is $\sim 2.7\%$ ($\sim 3.2\%$) for the linearized (exact) expressions. These differences are small and generally within the uncertainties in the calculation of energies. In addition, the Virial theorem provides consistently slightly higher total energies for NOAA AR 8844, while it consistently provides slightly lower total energies for NOAA AR 9165. This mixed behavior, as well as the source of the slight discrepancy in total energies, are unclear. One possible reason may be the application of Fourier transforms, and hence an implicit assumption of periodic boundary conditions, in analytical expressions where fields are required to vanish at infinity. Why this does not have an impact in the calculation of the potential energy is also unclear. Nevertheless, the small

discrepancies prompt us to conclude that our energy expressions are consistent with the Virial theorem. The reasons why we have derived and used them instead of the latter are that (i) they provide a self-consistent description of the energy *and* helicity budgets, and (ii) they are physically intuitive, derived from first principles, and, hopefully, capable of being generalized for NLFF magnetic fields.

6. Summary and discussion

The reliable calculation of the magnetic energy and helicity budgets in the active-region solar corona is an essential step toward the quantitative understanding of solar eruptions and has profound space-weather applications. Our goal is to derive a practical set of equations that are applicable to solar vector magnetograms and can evaluate the magnetic energy and relative magnetic helicity budgets in a physically intuitive, self-consistent manner. Here we provide expressions for the magnetic energy and relative helicity budgets in case of a constant-alpha, flux-balanced, magnetic structure, thus implementing the LFF approximation. These equations are to be generalized into magnetic structures with non-constant alpha values, thus implementing the NLFF approximation. This objective will be pursued in a later study.

To perform our LFF analysis we separately derive each of the terms present in the energy-helicity formula of Berger (1988), namely the total magnetic energy, the potential magnetic energy, and the relative magnetic helicity related to the free magnetic energy, together with their uncertainties. Our analysis unifies numerous expressions for the relative helicity and links several virtually unconnected studies into a self-consistent energy-helicity description that is practical enough to be applied to vector magnetograms of solar active regions. For the ground-state, potential, magnetic energy we provide a general surface-integral expression, equation (14). This expression gives results practically identical to those of the magnetic Virial theorem. The potential magnetic energy is then used as a free parameter to explicitly determine the total and free magnetic energy, as well as the relative magnetic helicity. The variable relating the potential energy to the free energy and the relative helicity has been calculated in two ways - an exact and a linearized one - by using and extending the analysis of Berger (1985). As a result, the magnetic energy and helicity budgets are calculated self-consistently as *surface integrals*, equations (35) - (37). This development reduces significantly the required computations. Reliability and computational speed are essential elements of a future real-time or near real-time calculation of the magnetic energy and helicity budgets in solar active regions.

To test our derivations we used three different types of semi-analytical LFF magnetic dipoles (§4.3). The conventional volume-integral expression for the relative magnetic helic-

ity was compared with our exact and linearized surface-integral expressions. The convincing match between the volume- and surface-integral helicity expressions for all models implies that our formulations are model-independent. Moreover, as expected from the analysis, the linearized surface-integral expression of the relative magnetic helicity, equation (37b), consistently provides a lower limit of the helicity present in the magnetic structures, with this behavior being more pronounced for large alpha values. For smaller alpha, all helicity expressions give nearly identical results. By extension, the linearized surface-integral expressions provide reasonable lower limits of the total and free magnetic energy, equations (35b) and (36b), respectively. Given also the convenient calculation of uncertainties in the linearized case, equations (38b) - (40b), we conclude that linearization is preferable over using the exact formulas, where alpha can resonate with the value of $(2\pi/L)$ and hence lead to infinite energies and helicities, as is well-known for LFF magnetic structures.

Two series of solar vector magnetograms, one for an eruptive and another for a noneruptive active region, were thereafter subjected to our analysis (§5). Both the exact and linearized expressions for the energy and helicity were used. We found that the exact expressions tend to give more spiky temporal evolutions and hence larger uncertainties in temporal averages, which provides an additional reason for preferring the linearized energy/helicity expressions in observations. Both ARs happened to exhibit nearly the same absolute alpha value. The eruptive active region, however, included several times more magnetic flux than the noneruptive AR. This effect was greatly amplified when the free magnetic energies and relative magnetic helicities of the two active regions were calculated and compared. This leads us to the conclusion that comparing the free energies and helicities might be a safe (safer than simply calculating the total magnetic flux) way of distinguishing between eruptive and noneruptive active regions⁴. The crucial point, however, is the *reliable* calculation of free energies and helicities. The LFF approximation is certainly not very reliable, as can be seen from the large error bars accompanying our free energy and helicity estimates ($\sim 45\%$ - 70%). To reach sound conclusions, the analysis involving and comparing free magnetic energies / relative magnetic helicities must be applied to statistically significant samples of active regions, and ideally by utilizing the NLFF approximation.

The force-free approximation is a prerequisite for our analysis because it is a very difficult, if not intractable, problem to perform non-force-free calculations of the nonpotential magnetic energy and the magnetic helicity in active regions. The only hope for non-force-free energy and helicity calculations emerges from data-driven three-dimensional magnetohydrodynamical (3D MHD) simulations of the active-region corona (e.g. Abbett 2003; Rousev et

⁴For an alternative criterion, based on the magnetic connectivity in solar active regions, see Georgoulis & Rust (2007).

al. 2004) which, however, require immensely time-consuming calculations. 3D MHD models are certainly capable of advancing our physical understanding of solar eruptions but, because of their intense computations, they cannot contribute to a real-time, or near real-time, space weather forecasting capability. Alternatively, non-force-free energy and helicity estimates can be obtained if an active region is continuously observed from its formation and thereafter. In this case, total energies and helicities can be calculated by temporally integrating the Poynting flux and magnetic helicity injection rate, respectively. If the birth of an active region is not observed, then the initial energy and helicity can only be assumed. In any case, both the Poynting flux and the helicity injection rate require the flow velocity of the magnetized plasma on the boundary of the magnetic field measurements. Inferring a *reliable* flow velocity is a completely independent, as well as highly nontrivial, problem (for a review, see Welsch et al. 2007).

Our force-free equations are physically better suited to apply to chromospheric, rather than photospheric, vector magnetograms. It has yet to be established whether the NLFF approximation holds for the active-region chromosphere (see Metcalf et al. [1995] in conjunction with Socas-Navarro [2005]) but it is almost certainly more valid there than in the photosphere. The first high-quality chromospheric vector magnetograms have already been obtained (the above authors as well as Leka & Metcalf 2003; Metcalf, Leka, & Mickey 2005; Wheatland & Metcalf 2006) but a routine acquisition and reduction of such data may still be a task for the future. In brief, force-free equations may be applied to photospheric vector magnetograms as a zero-order (LFF) or first-order (NLFF) approximation, but one expects larger uncertainties in the values of energy and helicity budgets, than when chromospheric vector magnetograms are used.

Concluding, we emphasize that the present analysis cannot fully uncover the importance of magnetic helicity in solar eruptions. Here we only show two examples that appear to point to this direction but an answer would require large numbers of active regions and NLFF energy/helicity equations, as already said. Our objective here was to calculate the relative magnetic helicity in active regions as an integral part of the energetics and complexity of the studied magnetic structures. It would be an important leap forward if it was convincingly shown that flare- and CME-prolific active regions exhibit significant quantitative differences in their free magnetic energy and/or total relative helicity (large free magnetic energy does not necessarily imply a large total relative magnetic helicity because roughly equal and opposite amounts of helicity may be simultaneously present - see Phillips, MacNeice, & Antiochos [2005]) compared to quiescent ARs. Intriguing clues to this direction stem from the study of the structural magnetic complexity in solar active regions (e.g. Georgoulis 2005b; Abramenko 2005) or the calculation of the free magnetic energy in active regions with exceptional flare and CME records (Metcalf, Leka, & Mickey 2005) but the role of

helicity is yet to be uncovered. Some pieces of evidence suggesting the importance of helicity in solar eruptions stem from the frequent presence of sigmoids in eruptive active regions (Rust & Kumar 1996; Canfield, Hudson, & McKenzie 1999), apparently due to significant amounts of helicity with a *prevailing* sign, the presence of large and highly variable alpha values in eruptive active regions (Nindos & Andrews 2004), and the statistical correlation between large helicity injection rates and X-class flares/CMEs (LaBonte, Georgoulis, & Rust 2007). Our forthcoming NLFF analysis will be well suited to address the role of helicity in solar eruptions and we intend to carry out this study in the future.

This work is dedicated to the memory of its co-author, Barry J. LaBonte. Barry is remembered as a deeply knowledgeable, distinguished colleague and an inspiring mentor. I am grateful to D. M. Rust for our continuous interaction on magnetic helicity in the Sun and for a critical reading of the manuscript. I also thank A. Nindos and S. Régnier for clarifying discussions on helicity issues and an anonymous referee whose numerous critical comments and suggestions resulted in substantial improvements in the paper. Partial support for this work has been received by NASA Grants NAG5-13504 and NNG05-GM47G.

A. Equivalence of equations (24) and (25) for the energy-helicity formula in the linear force-free approximation

To show that equations (24) and (25) are equivalent in the LFF approximation, it is sufficient to show that the potential energy E_p is given by

$$E_p = \frac{1}{8\pi} \int_S \mathbf{B} \times \mathbf{A}_p \cdot \hat{\mathbf{z}} dS \quad , \quad (\text{A1})$$

for any LFF magnetic field $\mathbf{B} \neq \mathbf{B}_p$.

We first decompose \mathbf{B} in equation (A1) into its potential (poloidal) and nonpotential (toroidal) components, \mathbf{B}_p and \mathbf{B}_c . Then, equation (A1) becomes

$$E_p = \frac{1}{8\pi} \int_S \mathbf{B}_p \times \mathbf{A}_p \cdot \hat{\mathbf{z}} dS + \frac{1}{8\pi} \int_S \mathbf{B}_c \times \mathbf{A}_p \cdot \hat{\mathbf{z}} dS \quad . \quad (\text{A2})$$

The first integral of equation (A2) is already the potential energy as shown in equation (14). To prove equation (A1), therefore, it is sufficient to show that

$$\int_S \mathbf{B}_c \times \mathbf{A}_p \cdot \hat{\mathbf{z}} dS = 0 \quad . \quad (\text{A3})$$

From $\mathbf{B}_p \cdot \mathbf{B}_c = 0$, we construct the volume integral $\int_{\mathcal{V}} \mathbf{B}_p \cdot \mathbf{B}_c d\mathcal{V} = 0$. Substituting the definition of \mathbf{A}_p from equation (5a) into this volume integral, we find after some analysis that

$$\int_{\partial\mathcal{V}} \mathbf{A}_p \times \mathbf{B}_c \cdot \hat{\mathbf{n}} d\sigma = - \int_{\mathcal{V}} \mathbf{A}_p \cdot \nabla \times \mathbf{B}_c d\mathcal{V} . \quad (\text{A4})$$

Taking into account that (i) \mathbf{A}_p vanishes at infinity, and (ii) $\nabla \times \mathbf{B}_c = \nabla \times \mathbf{B}$, because $\nabla \times \mathbf{B}_p = 0$, equation (A4) further reduces to

$$\int_{\mathcal{S}} \mathbf{B}_c \times \mathbf{A}_p \cdot \hat{\mathbf{z}} d\mathcal{S} = - \int_{\mathcal{V}} \mathbf{A}_p \cdot \nabla \times \mathbf{B} d\mathcal{V} . \quad (\text{A5})$$

In the LFF approximation, however, $\nabla \times \mathbf{B} = \alpha \mathbf{B}$, with α constant, so equation (A5) gives

$$\int_{\mathcal{S}} \mathbf{B}_c \times \mathbf{A}_p \cdot \hat{\mathbf{z}} d\mathcal{S} = -\alpha \int_{\mathcal{V}} \mathbf{A}_p \cdot \mathbf{B} d\mathcal{V} . \quad (\text{A6})$$

Given the gauge-invariant definition of the relative magnetic helicity, however, it can be shown (Berger 1988; 1999) that

$$\int_{\mathcal{V}} \mathbf{A}_p \cdot \mathbf{B} d\mathcal{V} = 0 . \quad (\text{A7})$$

Combining equations (A6) and (A7) we obtain equation (A3). Therefore, equation (A1) is true and hence equations (24) and (25) in §3 are equivalent as asserted.

B. Derivation of the variable linking the potential and the total magnetic energy in the LFF approximation

Here we will derive the form of the dimensionless variable f in equation (32). This variable links the total and the free magnetic energies in a constant-alpha magnetic structure. We will use and extend the analysis performed in Appendix AII of Berger (1985). Assuming planar geometry, Berger (1985) utilized Chandrasekhar's (1956; 1961) decomposition of an arbitrary magnetic field vector into a poloidal and a toroidal components and, in view of the LFF approximation, he derived the total magnetic energy and the relative magnetic helicity.

Following Berger (1985), the total magnetic energy of the structure is given by

$$E = \frac{\pi}{2} \sum_{l=1}^{n_x} \sum_{m=1}^{n_y} \frac{|b_{u_l, v_m}^2|}{k_{l,m}} , \quad (\text{B1})$$

where b_{u_l, v_m} is the Fourier amplitude of the vertical magnetic field B_z for the harmonic (u_l, v_m) in a two-dimensional Fourier space with linear dimensions n_x, n_y . In addition, we

have $k_{l,m}^2 = u_l^2 + v_m^2 - \alpha'^2$. The force-free parameter α' is expressed in inverse length units (i.e., $1/x$, where x is the number of unit lengths required for $\alpha' = 1$) and not in physical units. This is why it is represented by α' , while the α used so far refers to the force-free parameter expressed in physical units. Typically, $\alpha' = \alpha d$, where d is the unit length expressed in physical units. Berger (1985) assumes periodic boundary conditions and a length unit of $[L/(2\pi)]$, where L is the linear dimension of the magnetic structure on the boundary \mathcal{S} . Moreover, $u_l = (2\pi l/L)$ and $v_m = (2\pi m/L)$. Then, the direct and inverse Fourier transform of B_z can be performed on \mathcal{S} only so that one can write

$$B_z(x, y)|_{\mathcal{S}} = \sum_{l=1}^{n_x} \sum_{m=1}^{n_y} b_{u_l, v_m} e^{i(u_l x + v_m y)} . \quad (\text{B2})$$

The required boundary conditions for b_{u_l, v_m} in order to have a real and finite magnetic energy and helicity is $b_{u_l, v_m} = 0$ for $\sqrt{u^2 + v^2} \leq |\alpha'|$ (see also Alissandrakis 1981).

Assuming that the magnetic structure does not include electric currents ($\alpha' = 0$), then equation (B1) provides the potential magnetic energy of the structure, namely

$$E_p = \frac{\pi}{2} \sum_{l=1}^{n_x} \sum_{m=1}^{n_y} \frac{|b_{u_l, v_m}^2|}{q_{l,m}} , \quad (\text{B3})$$

where $q_{l,m}^2 = u_l^2 + v_m^2$.

From equation (32), the variable f is given by the dimensionless ratio

$$f = \frac{E - E_p}{E_p} . \quad (\text{B4})$$

Substituting equations (B1) and (B3) into equation (B4) we obtain

$$f = \frac{\sum_u \sum_v |b_{u,v}^2| \frac{q-k}{kq}}{\sum_u \sum_v \frac{|b_{u,v}^2|}{q}} , \quad (\text{B5})$$

where we have denoted $\sum_{l=1}^{n_x} \sum_{m=1}^{n_y}$ by $\sum_u \sum_v$ for simplicity. The ratio of sums in equation (B5) depends on α' because of its dependence on k . This dependence can cause problems when $|\alpha'| \rightarrow (2\pi/L)$ because $k \rightarrow 0$ for $l = m = 1$ in this case and f becomes infinite. This problem is not new; that LFF fields sometimes give solutions that are not fully specified by the boundary condition and may include infinite energy has been explicitly acknowledged by Alissandrakis (1981), but also by Chiu & Hilton (1977), using a different analytical framework. Clearly, this is a caveat of the LFF approximation and restricts its applicability. To avoid infinite energy values when $|\alpha'| \rightarrow (2\pi/L)$, equation (B5) can be linearized with

respect to α'^2 , assuming small values of α' . We first write $(q - k)/(kq) = (q^2 - kq)/(kq^2)$. Expanding $q^2 - kq$ in a MacLaurin series, one finds $q^2 - kq \simeq (q^2 - k^2)/2 = \alpha'^2/2$. Moreover, for $|\alpha'| \ll \sqrt{2}2\pi/L$, one finds $kq^2 \simeq q^3$. Then, the linearized equation (B5) becomes

$$f_l = \frac{\alpha'^2}{2} \frac{\sum_u \sum_v \frac{|b_{u,v}^2|}{q^3}}{\sum_u \sum_v \frac{|b_{u,v}^2|}{q}} . \quad (\text{B6})$$

Berger (1985) goes further on to derive a linearized expression for the total relative magnetic helicity in the volume \mathcal{V} above \mathcal{S} , namely

$$H_m = 4\pi^2 \alpha' \sum_u \sum_v \frac{|b_{u,v}^2|}{kq^2} . \quad (\text{B7})$$

Although not explicitly mentioned in Berger's (1985) analysis, equation (B7) appears to occur by assuming that $q^2 - kq \simeq \alpha'^2$, instead of $q^2 - kq \simeq \alpha'^2/2$, that we have assumed in equation (B6). In our formulation, therefore, Berger's (1985) equation (B7) is a factor of two too high. If no linearization is performed, then our equation (B5) is in agreement with Berger's (1985) analysis.

In an observed vector magnetogram, the best α -value is inferred in physical units of inverse length. The scaled value α' of the force-free parameter relates to α via the equation $\alpha' = \alpha d$ where d is the elementary length in the magnetogram, expressed in physical units. As in any discrete parameter distribution with a well-defined (preferably fixed) length element, the length d in the magnetogram can be naturally represented by the linear size of the magnetogram's pixel. From this understanding and using the definition $q^2 = u^2 + v^2$, the linearized expression f_l for f can be written as

$$f_l = \mathcal{F}_l d^2 \alpha^2 \quad \text{where} \quad \mathcal{F}_l = \frac{1}{2} \frac{\sum_u \sum_v \frac{|b_{u,v}^2|}{(u^2+v^2)^{3/2}}}{\sum_u \sum_v \frac{|b_{u,v}^2|}{(u^2+v^2)^{1/2}}} . \quad (\text{B8})$$

It is important to emphasize that the linearization f_l as shown in equation (B8) provides a lower limit of f , and hence a lower limit of the free magnetic energy E_c and the relative magnetic helicity H_m in the LFF approximation (equations (35) - (37)). Green et al. (2002) and Démoulin et al. (2002) reached the same conclusion when deriving the linearized helicity expression of equation (2). Since the LFF magnetic energy is the minimum energy for a given relative helicity (a consequence of the Woltjer-Taylor theorem), the linearized energy/helicity expressions are underestimations of the actual energy/helicity values. The underestimation of E_c and H_m is negligible for small values of $|\alpha'|$ and increases as $|\alpha'| \rightarrow (2\pi/L)$. This, however, does not invalidate the linearized energy/helicity expressions for larger $|\alpha'|$. As

we see in Figure 1b, the underestimation factor is reasonable even for large $|\alpha'|$, at least in view of other sources of uncertainties that are expected for observed magnetic configurations, and especially the use of the LFF approximation itself. Démoulin (2006), also provides a practical explanation of the underestimation effect based on well-known properties of the LFF magnetic fields.

REFERENCES

- Abbett, W. P., 2003, Fall AGU Meeting, abstract #SM11A-03
- Abramenko, V. I., 2005, *ApJ*, 629, 1141
- Alissandrakis, C. E., 1981, *A&A*, 100, 197
- Aly, J. J., 1984, *ApJ*, 283, 349
- Antiochos, S. K., & DeVore, C. R., 1999, in *Magnetic Helicity in Space and Laboratory Plasmas*, ed. M. R. Brown, R. C. Canfield, & A. A. Pevtsov, Geophysical Monograph 11, 187
- Berger, M. A., 1985, *ApJS*, 59, 433
- Berger, M. A., 1988, *A&A*, 201, 355
- Berger, M. A., 1999, *Plasma Phys. Contr. Fusion*, 41(12B), 167
- Berger, M. A., & Field, G. B., 1984, *J. Fluid Mech.*, 147, 133
- Berger, M. A., & Ruzmaikin, A., 2000, *JGR*, 105(A5), 10481
- Bernasconi, P. N., Rust, D. M., and Eaton, H. A. C., 2001, in *Advanced Advanced Solar Polarimetry - Theory, Observation, and Instrumentation* (ed.: Sigwarth, M.), ASP Conf. Series, 236, 399
- Călugăreanu, G., 1961, *Czechoslovak Math. J.*, 11, 588
- Canfield, R. C., Hudson, H. S., & McKenzie, D. E., 1999, *GRL*, 26, 627
- Chae, J., 2001, *ApJ*, 560, L95
- Chandrasekhar, S., 1956, *Proc. Nat. Acad. Sci*, 42, 1

- Chandrasekhar, S., 1961, *Hydrodynamic and Hydromagnetic Stability* (Oxford University Press: Oxford), p. 622
- Chiu, Y. T., & Hilton, H. H., 1977, *ApJ*, 212, 873
- Démoulin, P., 2006, *Adv. Space Res.*, submitted
- Démoulin, P., Mandrini, C. H., van Driel-Gesztelyi, L., Thompson, B. J., Plunkett, S., Kovári, Zs., Aulanier, G., & Young, A., 2002, *A&A*, 382, 650
- Dixon, A. M., Berger, M. A., Browning, P. K., & Priest, E. R., 1989, *A&A*, 225, 156
- DeVore, R. C., 2000, *ApJ*, 539, 944
- Devore, R. C., & Antiochos, S. K., 2005, *ApJ*, 628, 1031
- Finn, J. H., & Antonsen, T. M., 1985, *Comm. Plasma Phys. Contr. Fusion*, 9, 111
- Gary, G. A., 1989, *ApJS*, 69, 323
- Gary, G. A., & Hagyard, M. J., 1990, *Sol. Phys.*, 126, 21
- Georgoulis, M. K., 2005a, *ApJ*, 629, L69
- Georgoulis, M. K., 2005b, *Sol. Phys.*, 228, 5
- Georgoulis, M. K., & LaBonte, B. J., 2004, *ApJ*, 615, 1029
- Georgoulis, M. K., & Rust, D. M., 2007, *ApJ Letters*, in press
- Gold, T., & Hoyle, F., 1960, *MNRAS*, 120, 89
- Green, L. M., López Fuentes, M. C., Mandrini, C. H., Démoulin, P., van Driel-Gesztelyi, L., & Culhane, J. L., 2002, *Sol. Phys.*, 208, 43
- Hagino, M., & Sakurai, T., 2004, *PASJ*, 56, 831
- Klimchuk, J. A., Canfield, R. C., & Rhoads, J. E., 1992, *ApJ*, 385, 327
- Kusano, K., Suzuki, Y., Kubo, H., Miyoshi, T., & Nishikawa, K., 1994, *ApJ*, 433, 361
- LaBonte, B. J., Mickey, D. L., & Leka, K. D., 1999, *Sol. Phys.*, 189, 1
- LaBonte, B. J., Georgoulis, M. K., & Rust, D. M., 2007, *ApJ*, submitted
- Landolfi, M., & degl’Innocenti, E. L., 1982, *Sol. Phys.*, 78, 355

- Leka, K. D., 1999, *Sol. Phys.*, 188, 21
- Leka, K. D., Canfield, R. C., McClymont, A. N., & van Driel-Gesztelyi, L., 1996, *ApJ*, 462, 547
- Leka, K. D., & Metcalf, Th. R., 2003, *Sol. Phys.*, 212, 361
- Leka, K. D., & Skumanich, A., 1999, *Sol. Phys.*, 188, 3
- Longcope, D. W., 2005, *Living Rev. Sol. Phys.*, 2, 7
- Low, B. C., 1994, *Phys. Plasmas*, 1(5), 1684
- Metcalf, Th. R., Jiao, L., McClymont, A. N., Canfield, R. C., & Uitenbroek, H., 1995, *ApJ*, 439, 474
- Metcalf, Th. R., Leka, K. D., Barnes, G., Lites, B. W., Georgoulis, M. K., Pevtsov, A. A., Gary, G. A., Jing, J., Balasubramaniam, K. S., Li, J., Liu, Y., Wang, H. N., Abramenko, V., Yurchyshyn, V., & Y.-J. Moon, 2006, *SoPh*, 237, 267
- Metcalf, Th. R., Leka, K. D., & Mickey, D. L., 2005, *ApJ*, 623, L53
- Mickey, D. L., Canfield, R. C., LaBonte, B. J., Leka, K. D., Waterson, M. F., & Weber, H. M., 1996, *Sol. Phys.*, 168, 229
- Moffatt, H. K., & Ricca, R. L., 1992, *Proc. R. Soc. London A*, 439, 411
- Molodensky, M. M., 1974, *SoPh*, 39, 393
- Nindos, A. 2006, in *Recent Advances in Astronomy and Astrophysics: 7th International Conference of the Hellenic Astronomical Society* (ed. N. H. Solomos), *AIP Conf. Proc.*, 848, 64
- Nindos, A., & Andrews, M. D., 2004, *ApJ*, 616, L175
- Pariat, E., Aulanier, G., Schmieder, B., Georgoulis, M. K., Rust, D. M., & Bernasconi, P. N., 2004, *ApJ*, 614, 1099
- Pevtsov, A. A., Canfield, R. C., & Metcalf, Th. R., 1995, *ApJ*, 440, L109
- Phillips, A. D., MacNeice, P. J., & Antiochos, S. K., 2005, *ApJ*, 624, L129
- Régnier, S., Amari, T., & Canfield, R. C., 2005, *A&A*, 442, 345

- Roussev, I. I., Sokolov, I. V., Forbes, T. G., Gombosi, T. I., Lee, M. A., & Sakai, J. I., 2004, *ApJ*, 605, L73
- Rust, D. M., 1994a, *GRL*, 21, 241
- Rust, D. M., 1994b, in *Solar Active Region Evolution: Comparing Models with Observations*, ed. Balasubramaniam, K. S., & Simon, G. W., *ASP Conf. Series*, 68, 335
- Rust, D. M., 2003, *Adv. Space Res.*, 32(10), 1895
- Rust, D. M., & Kumar, A., 1996, *ApJ*, 464, L199
- Rust, D. M., & LaBonte, B. J., 2005, *ApJ*, 622, L69
- Sakurai, T., 1981, *Sol. Phys.*, 69, 343
- Sakurai, T., & Uchida, Y., 1977, *Sol. Phys.*, 52, 397
- Schmidt, H. U., 1964, in *The Physics of Solar Flares*, ed. W. N. Hess (NASA SP-50; Washington, DC; NASA) 107
- Schmieder, B., Rust, D. M., Georgoulis, M. K., Démoulin, P., & Bernasconi, P. N., 2004, *ApJ*, 601, 530
- Schrijver, C. J., DeRosa, M. L., Metcalf, Th. R., Liu, Y., McTiernan, J., Régnier, S., Valori, G., Wheatland, M. S., & Wiegmann, Th., 2006, *SoPh*, 235, 161
- Socas-Navarro, H., 2005, *ApJ*, 631, L167
- Taylor, J. B., 1974, *Phys. Rev. Lett.*, 33, 1139
- Taylor, J. B., 1986, *Rev. Mod. Phys.*, 58(3), 741
- Welsch, B. T., Abbett, W. P., DeRosa, M. L., Fisher, G. H., Georgoulis, M. K., Kusano, K., Longcope, D. W., Ravindra, B., & Schuck, P. W., 2007, *ApJ*, submitted
- Wheatland, M. S., & Metcalf, Th. R., 2006, *ApJ*, 636, 1151
- Woltjer, L., 1958, *Proc. Nat. Acad. Sciences*, 44(6), 489

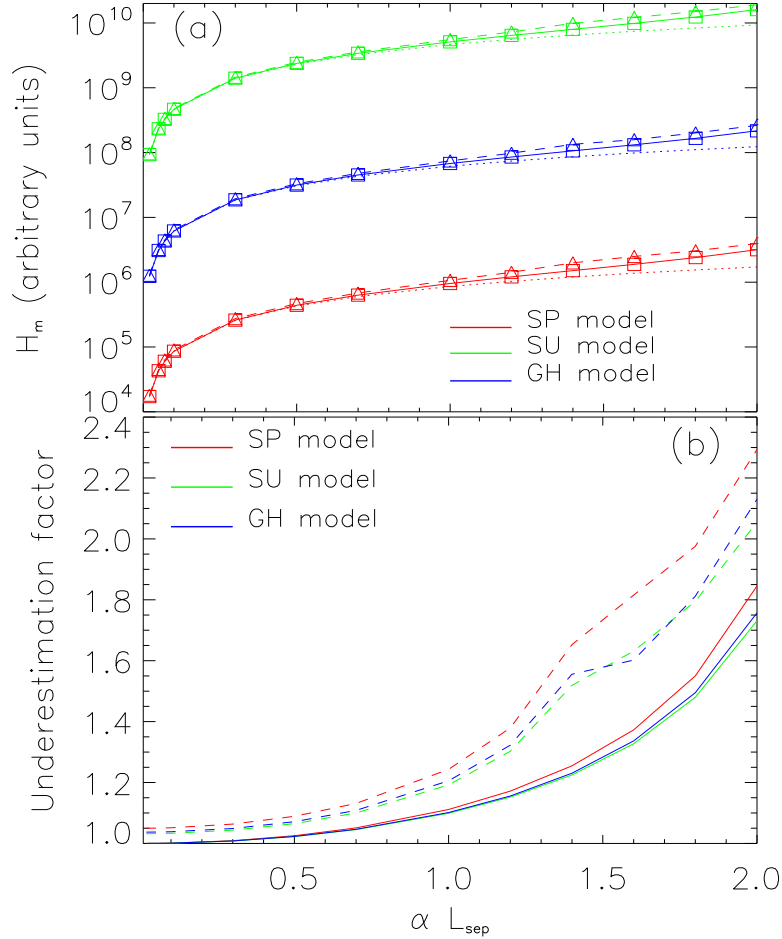


Fig. 1.— Comparison between the volume- and the surface-integral expressions of the relative magnetic helicity H_m in three LFF dipole models with analytical boundary conditions for the vertical magnetic field component. Boundary conditions are taken by the submerged poles (SP) model solution, the Sakurai-Uchida (SU) solenoidal model solution, and the Gold-Hoyle (GH) model solution (see §4.3 for details). Different model results are represented by different colors. (a) Dashed curves and triangles refer to results of the volume-integral helicity, equation (28), while the exact surface-integral results, equation (40a), are shown by solid curves and rectangles. The linearized surface-integral results, equation (40b), are shown by dotted curves. (b) Dashed curves refer to the ratios between the volume-integral helicity and the linearized surface-integral helicity, while solid curves show the ratios between the exact surface-integral helicity and the linearized surface-integral helicity for each of the models. In all cases, the footpoint separation length L_{sep} of the dipoles has been kept fixed.

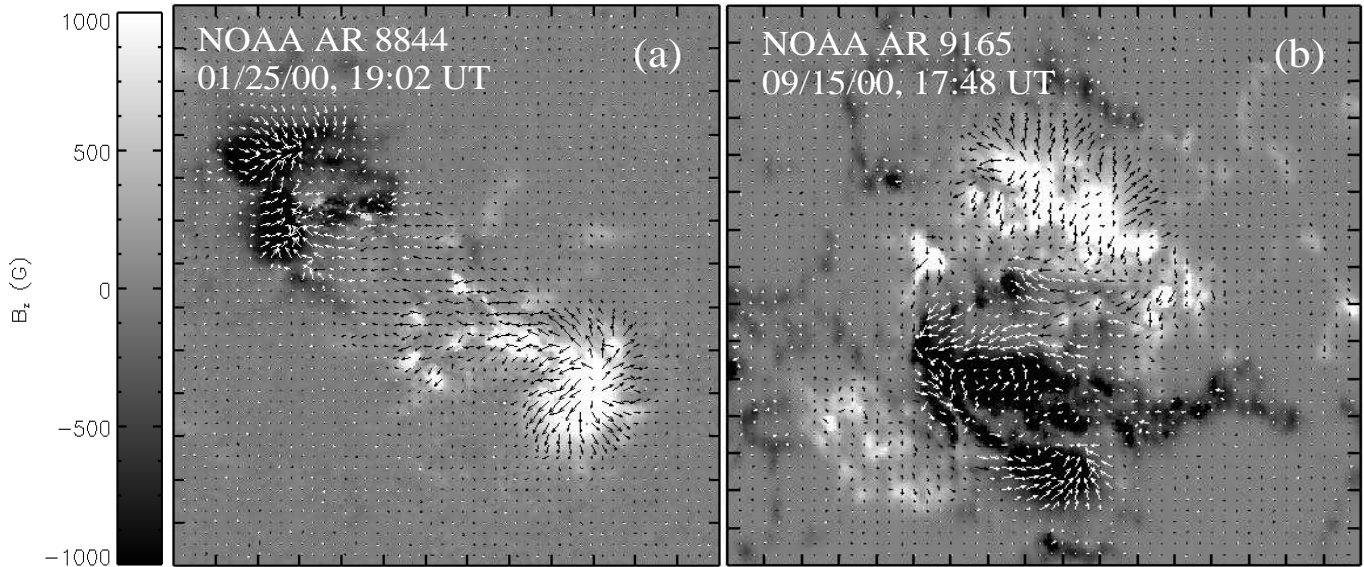


Fig. 2.— Parts of the magnetic configuration of the two studied solar ARs. Shown are the heliographic magnetic field components of the ARs on the heliographic plane. (a) Disambiguated photospheric vector magnetogram of NOAA AR 8844 as obtained by the IVM on 2000 January 25 at 19:02 UT. A vector length equal to the tick mark separation corresponds to a horizontal magnetic field of 2300 G . (b) Disambiguated photospheric vector magnetogram of NOAA AR 9165 as obtained by the IVM on 2000 September 15 at 17:48 UT. A vector length equal to the tick mark separation corresponds to a horizontal magnetic field of 1760 G . Tic mark separation in both images is $10''$. North is up; west is to the right.

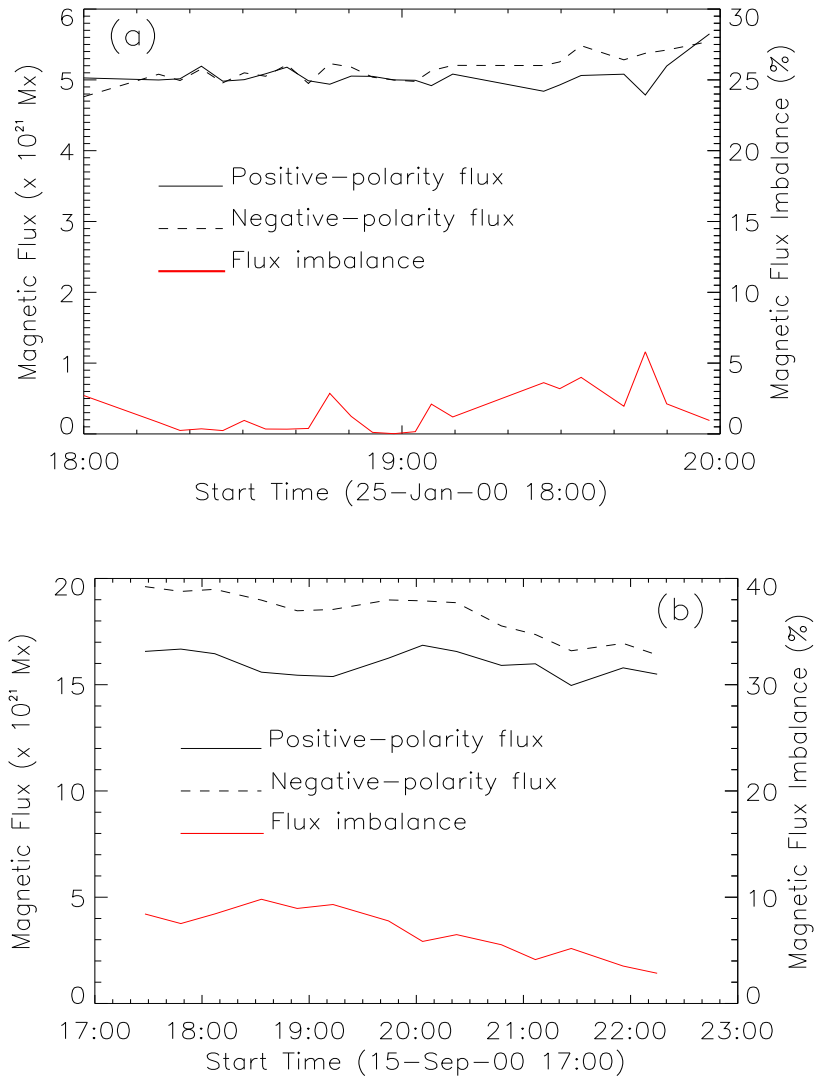


Fig. 3.— Timeseries of the magnetic flux and flux imbalance in the two studied ARs. Negative- (positive-) polarity fluxes are indicated by dashed (solid) curves, with readings on the left ordinate, while the red line corresponds to the relative magnetic flux imbalance in the ARs, with readings on the right ordinate. (a) NOAA AR 8844 (b) NOAA AR 9165.

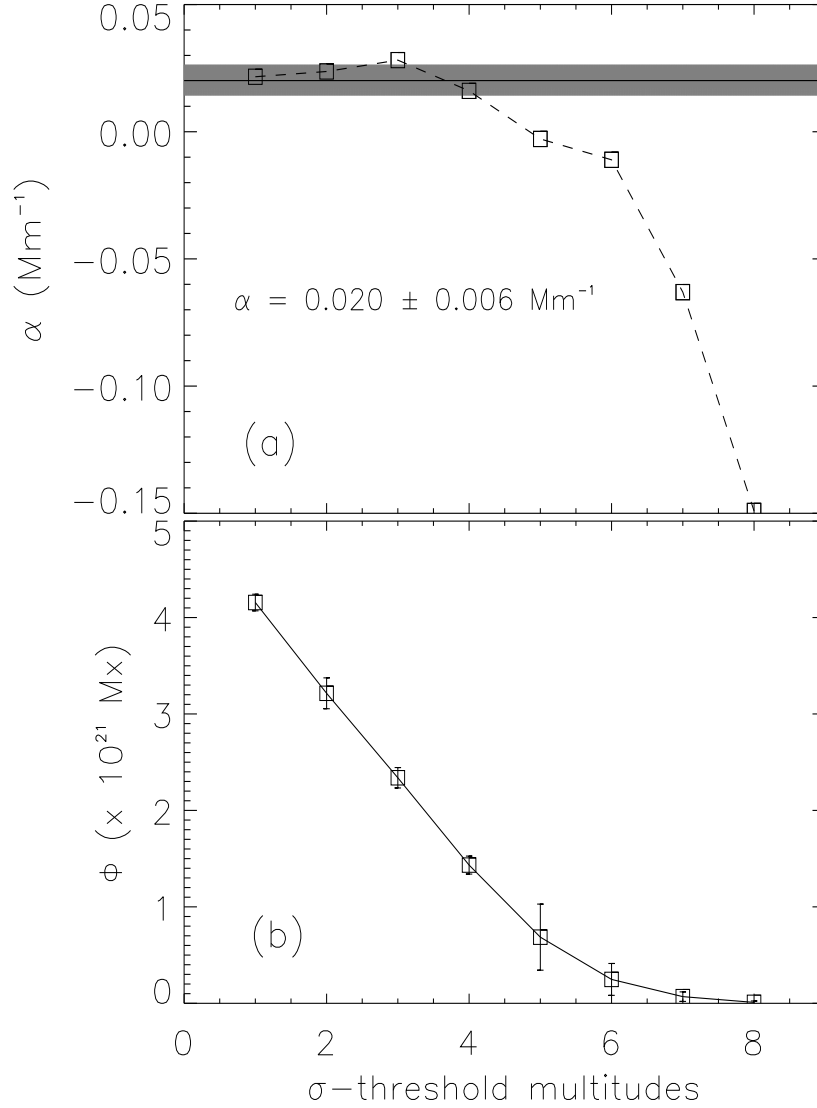


Fig. 4.— Example calculation of a unique α -value in NOAA AR 8844 for a vector magnetogram obtained at 18:18 UT on 2000 January 25. (a) Various α -values obtained for various significance thresholds σ (see text). The straight solid line indicates the flux-weighted average of these α -values and the shaded area indicates the uncertainty in the calculation of this average. (b) Estimates of the total unsigned magnetic flux in the AR for various significance thresholds σ . A threshold of 1σ corresponds to a vertical magnetic field of 100 G and a horizontal magnetic field of 200 G .

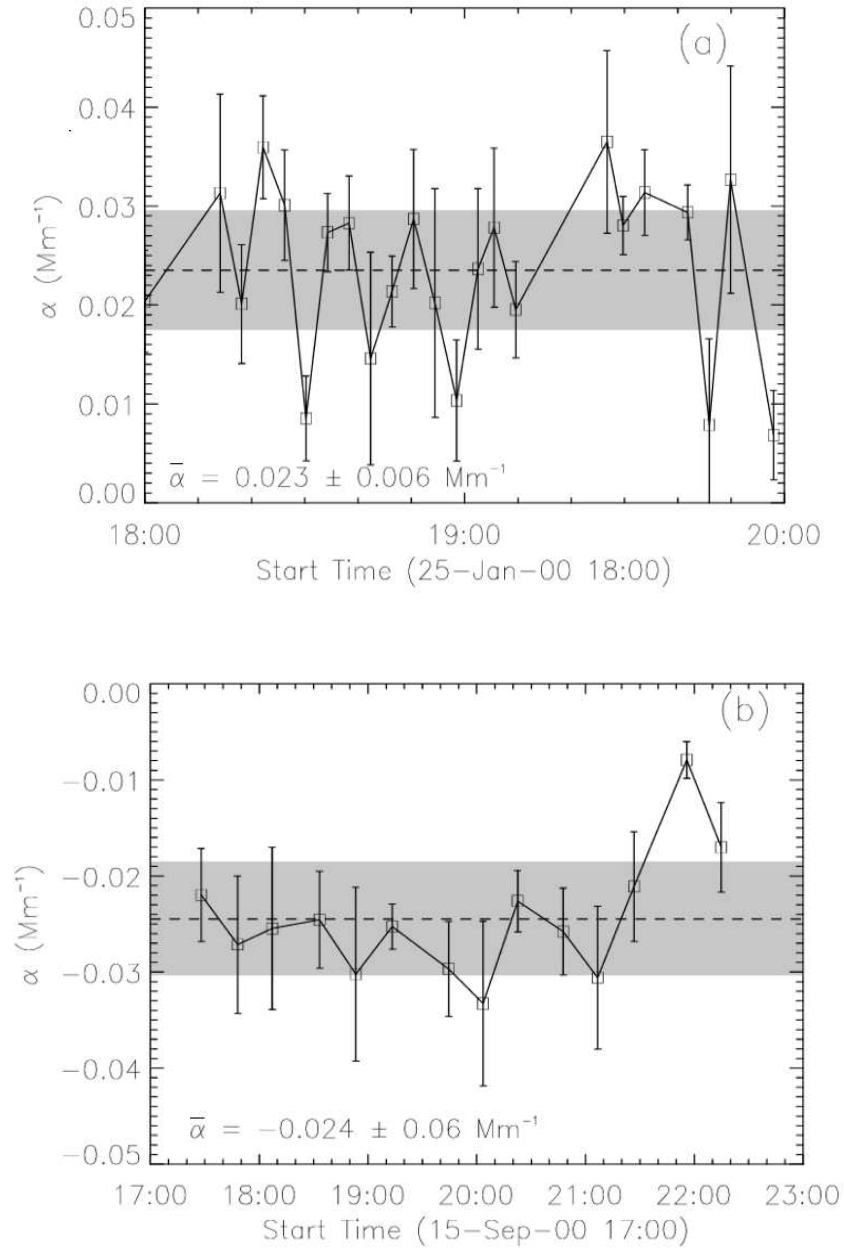


Fig. 5.— Timeseries of the constant force-free parameter α in the two studied ARs. The dashed line and the surrounding shaded area correspond to the estimated average α -value and its uncertainties, respectively. (a) NOAA AR 8844 (b) NOAA AR 9165.

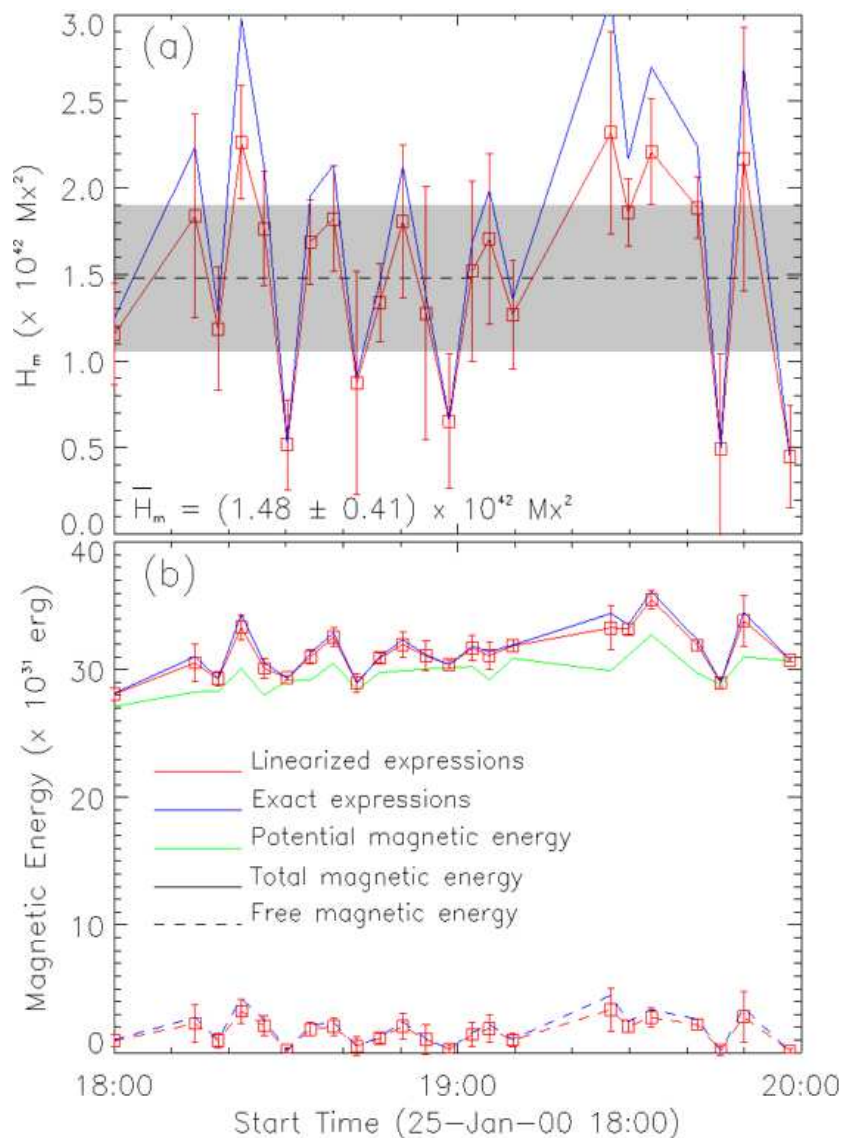


Fig. 6.— Magnetic energy and helicity budgets in NOAA AR 8844. Red (blue) curves correspond to the linearized (exact) surface-integral expressions. The error bars have been calculated from the linearized expressions. (a) Timeseries of the total relative magnetic helicity H_m . The dashed line and the surrounding shaded area correspond to the linearized average value and its uncertainties, respectively. (b) Timeseries of the magnetic energy budgets in the AR. The potential magnetic energy is shown by the green curve. The total (free) energy and its uncertainties are shown by the solid (dashed) curves.

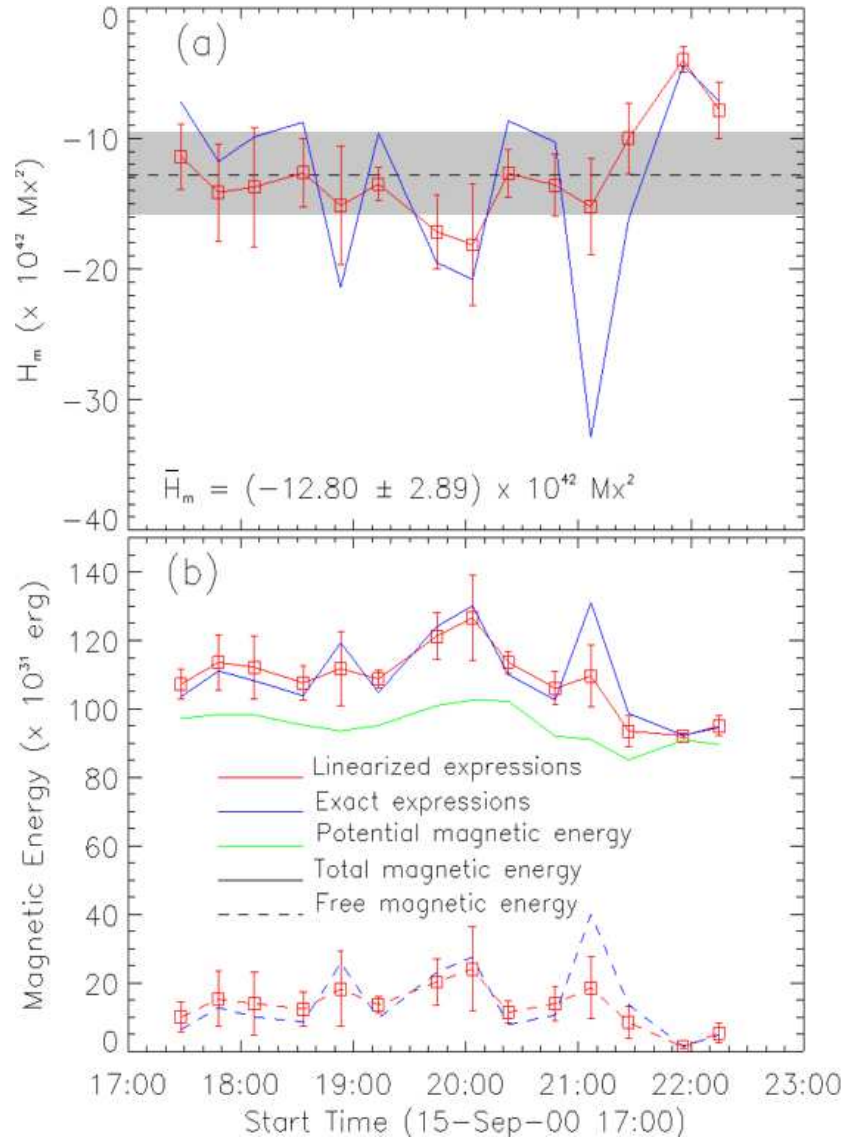


Fig. 7.— Same as Figure 6, but for NOAA AR 9165.

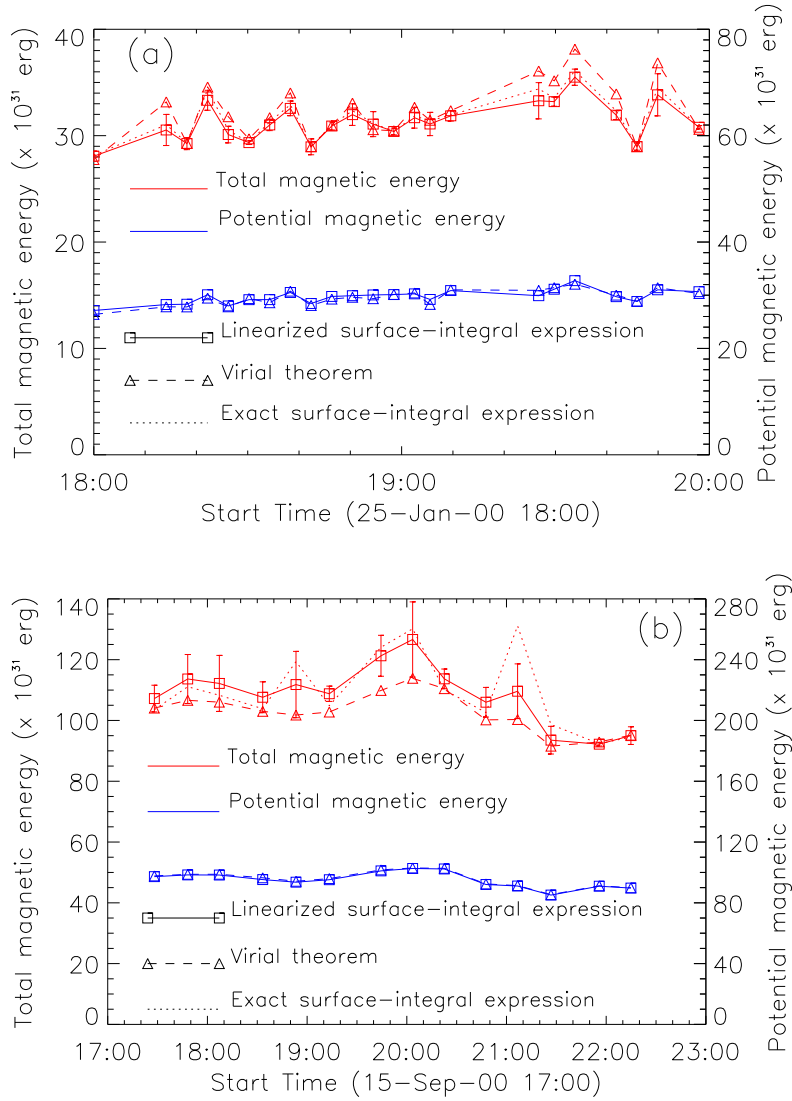


Fig. 8.— Comparison between the potential and the total magnetic energy estimates provided by our analysis (equations (14) and (38a), (38b)) and the Virial theorem (equation (22)) for the two studied ARs. Shown with blue (red) curves are the potential (total) magnetic energy estimates. The linearized (exact) estimates for the total energy are represented by solid curves and rectangles (dotted curves). The Virial-theorem estimates are represented by dashed curves and triangles. The error bars correspond to the linearized expression for the total energy. For clarity in comparing the different energy values, we have applied a different scaling for the total energy (with readings on the left ordinate) than the scaling for the potential energy (with readings on the right ordinate). (a) NOAA AR 8844. (b) NOAA AR 9165.

NOAA AR	$\bar{\Phi}$ ($\times 10^{21} Mx$)	$\bar{\alpha}$ (Mm^{-1})	\bar{H}_m ($\times 10^{42} Mx^2$)	
			Exact	Linearized
8844.....	5.1 ± 0.2	0.023 ± 0.006	1.73 ± 0.8	1.48 ± 0.4
9165.....	17.1 ± 0.8	-0.024 ± 0.006	-13.5 ± 7.8	-12.8 ± 3.7
Ratio.....	3.4 ± 0.06	1	7.8 ± 0.7	8.6 ± 0.5

Table 1: Synopsis of the average magnetic flux, α -value, and relative magnetic helicity budgets for NOAA ARs 8844 and 9165. The third row refers to the ratio $|P_{9165}/P_{8844}|$ between a given parameter P_{9165} of NOAA AR 9165 and the respective parameter P_{8844} of NOAA AR 8844.

NOAA AR	E_p ($\times 10^{32} erg$)	\bar{E}_c ($\times 10^{32} erg$)		\bar{E} ($\times 10^{32} erg$)	
		Exact	Linearized	Exact	Linearized
8844.....	2.97 ± 0.1	0.19 ± 0.13	0.15 ± 0.1	3.16 ± 0.2	3.13 ± 0.2
9165.....	9.52 ± 0.5	1.44 ± 1.1	1.33 ± 0.6	10.96 ± 1.2	10.85 ± 0.9
Ratio.....	3.2 ± 0.06	7.6 ± 1	8.9 ± 0.8	3.5 ± 0.2	3.5 ± 0.1

Table 2: Synopsis of the average potential, free, and total magnetic energy budgets, respectively, for NOAA ARs 8844 and 9165. The third row refers to the ratio (P_{9165}/P_{8844}) between a given parameter P_{9165} of NOAA AR 9165 and the respective parameter P_{8844} of NOAA AR 8844.